

1 **Collateral cleavage of 28s rRNA by RfxCas13d causes death of mice**

2 Yunfei Li^{1,7}, Junjie Xu^{2,3,7}, Xuefei Guo^{1,7}, Zhiwei Li^{4,7}, Lili Cao⁵, Shengde Liu⁶, Ying Guo²,
3 Guodong Wang², Yujie Luo¹, Zeming Zhang¹, Xuemei Wei¹, Yingchi Zhao¹, Tongtong Liu¹,
4 Xiao Wang¹, Huawei Xia¹, Ming Kuang¹, Qirui Guo¹, Junhong Li¹, Luoying Chen¹, Yibing
5 Wang², Qi Li², Fengchao Wang², Qinghua Liu^{2,*}, Fuping You^{1,*}

6 ¹ Institute of Systems Biomedicine, Department of Immunology, School of Basic Medical Sciences,
7 Beijing Key Laboratory of Tumor Systems Biology, Peking University Health Science Center, Beijing
8 100191, China.

9 ² National Institute of Biological Sciences, Beijing, Tsinghua Institute of Multidisciplinary Biomedical
10 Research, Tsinghua University, Beijing 102206, China.

11 ³ College of Life Sciences, Beijing Normal University, Beijing 100875, China.

12 ⁴ School of Life Sciences, Institute of Life Sciences and Green Development, Hebei University,
13 Baoding 071002, Hebei, China.

14 ⁵ Beijing Institutes of Life Science, Chinese Academy of Sciences, Beijing 100101, China.

15 ⁶ Department of Gastrointestinal Oncology, Key Laboratory of Carcinogenesis and Translational
16 Research (Ministry of Education/Beijing), Peking University Cancer Hospital and Institute, Beijing
17 100142, China.

18 ⁷ These authors contributed equally to this work.

19 * Correspondence: fupingyou@hsc.pku.edu.cn (F.Y.) and liuqinghua@nibs.ac.cn (Q.L.).

20 **Summary**

21 The CRISPR-Cas13 system is an RNA-guided RNA-targeting system, and has been widely used
22 in transcriptome engineering with potentially important clinical applications. However, it is still
23 controversial whether Cas13 exhibits collateral activity in mammalian cells. Here, we found that
24 knocking down gene expression using RfxCas13d in the adult brain neurons caused death of mice,
25 which was not resulted from the loss of target gene function or off-target effects. Mechanistically,
26 we showed that RfxCas13d exhibited collateral activity in mammalian cells, which is positively
27 correlated with the abundance of target RNA. The collateral activity of RfxCas13d could cleave
28 28s rRNA into two fragments, leading to translation attenuation and activation of the
29 ZAK α -JNK/p38-immediate early gene (IEG) pathway. These results provide new mechanistic
30 insights into the collateral activity of RfxCas13d and warn that the biosafety of CRISPR-Cas13
31 system needs further evaluation before applying it to clinical treatments.

32
33 **Keywords**

34 RfxCas13d, collateral activity, death of mice, 28s rRNA breakage

35

36 Introduction

37 Clustered regularly interspaced short-palindromic repeats (CRISPR) and accompanying
38 CRISPR-associated (Cas) proteins constitute the adaptive CRISPR-Cas immune system in bacteria
39 and archaea, which protects the bacteria from invaders, including phages and mobile genetic
40 elements. The defense process can be divided into three stages: Adaptation, incorporation of
41 foreign DNA fragments into CRISPR array as spacers; CRISPR RNA (crRNA) biogenesis,
42 CRISPR array is transcribed into a long precursor crRNA (pre-crRNA), and then processed into
43 mature crRNAs; Interference, Cas effector proteins, under the guidance of crRNAs, specifically
44 recognize and cleave foreign genetic elements. The rapid evolutionary arms race between bacteria
45 and mobile genetic elements has greatly enriched CRISPR-Cas systems, which have been
46 harnessed for various research and therapeutic applications. According to the structure and
47 function of Cas effector proteins, CRISPR-Cas systems can be categorized into two classes, which
48 are further subdivided into six types (type I-VI). Class 1 effectors comprise of multiple subunits,
49 including type I, II, and III, while class 2 effectors are single large proteins, including type IV, V
50 and VI^[1]. Due to their simplicity, Class 2 CRISPR-Cas systems have been widely developed as
51 genome editing and transcriptional regulating tools, such as DNA-targeting Cas9 and Cas12,
52 RNA-targeting Cas13.

53 Cas13 was originally found by mining microbial genome sequencing data using the highly
54 conserved adaption protein Cas1 as the anchor^[2]. Protein sequence alignments revealed that Cas13
55 contains two higher eukaryotes and prokaryotes nucleotide-binding (HEPN) domains and is
56 predicted to possess ribonuclease (RNase) activity^[2]. It was confirmed by subsequent experiments
57 that Cas13-crRNA complex recognizes and cleaves the target RNA via base pairing between the
58 crRNA and the target RNA^[3]. Surprisingly, binding of the target RNA to Cas13-crRNA complex
59 also activates a nonspecific RNase activity, which promiscuously cleaves bystander RNAs without
60 complementarity to the crRNA, leading to cell death or dormancy in bacteria^[3,4]. This activity was
61 referred as collateral activity of Cas13 and had been ingeniously developed as molecular diagnosis
62 tool *in vitro*^[5]. However, this collateral activity has not been detected in mammals. Theoretically,
63 compared with Cas9-mediated gene knockout technology, Cas13 can accurately distinguish
64 different transcripts of the same gene, and then study their function individually. Besides,
65 Cas13-mediated gene silencing does not change genomic DNA, so this gene silencing is reversible
66 and considered safer than Cas9, which has advantages over Cas9 in the treatment of some
67 acquired diseases. Moreover, accumulating evidence over the past decade highlights that
68 noncoding RNAs play important roles in various cellular processes. Cas13 is more suitable for
69 noncoding RNAs research than Cas9.

70 Currently, there are six subtypes identified in the Cas13 family, including Cas13a, Cas13b,
71 Cas13c, Cas13d, Cas13X and Cas13Y^[2, 6-10]. Since their discovery, Cas13's subtypes, such as
72 LwaCas13a, PspCas13b, RfxCas13d and Cas13X.1, have been widely used in knockdown
73 experiments in mammalian cells, exhibiting higher efficiency and specificity than traditional RNA
74 interference, and no collateral activity was detected^[3, 6, 8, 10]. Among these Cas13's subtypes, due to
75 its advantages in efficiency and size, RfxCas13d was applied in mammals via adeno-associated
76 virus (AAV) delivery, with no side-effects reported^[11-13]. But several research groups have
77 different opinions about collateral activity of Cas13. Kang group first reported that the collateral
78 activity of LwaCas13a occurred in U87 cells, non-specifically cleaving non-target RNAs, leading
79 to cell death^[14]. Later, they and collaborators reported that this phenomenon also existed in HepG2,
80 AT2, B16F10 and GL261 cells^[15, 16]. Following their work, Gootenberg and Abudayyeh group
81 reported that collateral activity was detected in U87 cells for LwaCas13a, PspCas13b and
82 RfxCas13d, and in HepG2 and mES cells for RfxCas13d^[17]. Yang group claimed that LwaCas13a,
83 RfxCas13d and Cas13X.1 exhibited collateral activity when targeting transiently overexpressing
84 mCherry, but not endogenous genes in 293T cells^[10]. Whereas, these studies did not figure out
85 what effect collateral activity of Cas13 has on mammalian cells. Therefore, it is still controversial
86 whether collateral activity of Cas13 exists in mammalian cells. More importantly, the safety of
87 applying Cas13 to treatment needs to be carefully evaluated in animal models.

88 Here, we found that mice died when using RfxCas13d to knock down genes in brain neurons.
89 The death would occur when target genes were present and obviously knocked down, but was not
90 due to loss of gene function or off-target effects, which narrows down to collateral activity of
91 Cas13. Then, we proved that RfxCas13d exhibited collateral activity in mammalian cells, which is

92 positively correlated with the abundance of target RNA. The collateral activity of RfxCas13d
93 cleaved 28s rRNA into two fragments, leading to translation attenuation and activation of the ZAK
94 α -JNK/p38-IEG pathway.
95

96 Results

97 Mice died when knocking down *Sik3-S* in neurons using RfxCas13d.

98 A recent study identified a *Sleepy* (*Sik3^{Sip/+}*) mouse strain, which carries a mutation in the gene
99 encoding salt-inducible kinase 3 (SIK3), a member of the AMP-activated protein kinase (AMPK)
100 family^[18]. The *Sleepy* (*Sik3^{Sip/+}*) mice exhibit over 4 h increase in daily non-rapid eye movement
101 sleep (NREMS) time and constitutively elevated NREMS delta power relative to wild-type (WT)
102 littermates^[18]. Interestingly, the *Sik3* gene encodes multiple transcripts due to alternative splicing.
103 Our recent study identified a new *Sik3-S* transcript encoding ~72 kDa short isoform of
104 SIK3^[19](Fig. S1a). To investigate the role of SIK3-S in sleep regulation, RfxCas13d was leveraged
105 to specifically knock down *Sik3-S* by taking advantage of its ability to distinguish different
106 transcripts of same gene (Fig. 1a). We designed eight crRNAs targeting *Sik3-S* and examined their
107 knockdown efficiency in N2a cells through RT-qPCR (Fig. S1b). Our results showed that, in
108 collaboration with RfxCas13d, all eight crRNAs, especially crRNA 1 and 8, caused significant
109 knockdown of *Sik3-S* expression (Fig. 1b). Transcriptome analysis revealed that *Sik3* was
110 specifically down-regulated while almost all the other genes remained unchanged when
111 RfxCas13d was co-transfected with *Sik3-S* crRNA 1 or 8, compared with non-targeting (NT)
112 crRNA (Fig. 1c).

113 We generated the ^{LSL}RfxCas13d knock-in mice by inserting the
114 CAG-loxP-STOP-loxP-RfxCas13d cassette into the *Rosa26* locus by homologous recombination
115 (Fig. S1c). To knock down *Sik3-S* expression in the adult brain neurons, we retro-orbitally injected
116 12-week-old ^{LSL}RfxCas13d adult mice with AAV-PHP.eB to deliver systemic expression of
117 U6-driven crRNA and hSYN-driven Cre (Fig. S1d). AAV-PHP.eB could efficiently cross the blood
118 brain barrier and transduced the majority of neurons and astrocytes across the adult mouse brain^[20].
119 The human synapsin 1 gene promoter (hSYN) restricted the expression of Cre recombinase in
120 neurons. Subsequently, Cre recombinase mediated excision of a tripartite transcriptional stop
121 cassette (STOP) flanked by loxP to release the expression of RfxCas13d. RfxCas13d, under the
122 guidance of *Sik3-S* crRNAs, specifically recognized and cleaved *Sik3-S* transcripts (Fig. 1d).
123 Unexpectedly, mice injected with AAV-PHP.eB containing *Sik3-S* crRNA 8 began to lose weight at
124 ~20 days post injection (dpi), and died at ~24 dpi (Fig. 1e-f). Brain lysates from *Sik3-S* crRNA 8
125 group, but not NT crRNA or *Sik3-S* crRNA 1 group, showed decreased SIK3-S expression,
126 demonstrating that *Sik3-S* expression was specifically knocked down in this group (Fig. 1g). This
127 phenomenon prevented our experiments from continuing, but aroused our curiosity-why mice died
128 when knocking down *Sik3-S* using RfxCas13d in the adult mouse brain neurons.

129

130 **RfxCas13d mediated lethality was not due to the loss of target gene function.**

131 Several previous studies have proved that RfxCas13d can be used to knock down endogenous
132 genes *in vivo* with no reported side-effects in liver, brain and eyes^[11-13]. In addition, although the
133 homozygous *Sik3* knockout mice can be created, but exhibit impaired chondrocyte during
134 development, neonatal lethality and reduced size, indicating that *Sik3* is essential for mouse health
135 and survival^[21, 22]. Therefore, we first guessed whether the death of mice was caused by
136 down-regulation of *Sik3-S*. To test this, we knocked out *Sik3* in the same neurons of mice by
137 conventional Cre-loxP system. We generated *Sik3-E5^{flox}* mice by inserting two loxP sites into both
138 sides of exon 5 in *Sik3* gene locus, and then delivered AAV-PHP.eB carrying hSYN-driven Cre
139 into *Sik3-E5^{flox}* mice to knock out *Sik3*, with WT mice as control (Fig. S2a). At 21 dpi, brain
140 lysates from *Sik3-E5^{flox}* mice showed lower SIK3-S expression level compared to WT mice (Fig.
141 2a). But *Sik3-E5^{flox}* mice behaved as normal as WT mice without loss of body weight or death
142 (Fig. 2b-c), which means that knocking out *Sik3* in neurons will not cause mouse death. Thus, the
143 mouse lethality that occurred when using RfxCas13d to knock down *Sik3-S* expression had
144 nothing to do with the loss of functional SIK3-S.

145 *Map2*, *Tau* and *NeuN* were well characterized neuron marker genes. Homozygous knockout of
146 each of these genes did not lead to death of mice^[23-25]. We thus selected them as targets and
147 knocked down each of three targets in the same way as knocking down *Sik3-S in vivo*. In theory,
148 when knocking down these genes individually using RfxCas13d in adult mouse brain neurons, the
149 mice will not die due to the loss of these genes. We designed six crRNAs for each gene and tested
150 their knockdown efficiency by RT-qPCR (Fig. 2d-e). Since N2a cells do not express *NeuN*, we
151 tested the efficiency of crRNAs by knocking down expression of co-transfected *NeuN* plasmid in
152 HEK293T (Fig. 2f). The two best crRNAs for each gene were selected for follow-up experiments.
153 Transcriptome analysis showed that these three genes were specifically knocked down using
154 corresponding crRNAs in tandem with RfxCas13d (Fig. 2g-i). Following the same protocol of
155 knocking down *Sik3-S in vivo*, we knocked down these three genes respectively in ^{LSL}RfxCas13d
156 mice. Results showed that mice in *Map2* crRNA 3, *Mapt* crRNA 6 and *Rbfox3* crRNA 5 groups
157 showed significant loss of body weight and death, while mice in the other groups behaved
158 normally and survived (Fig. 2j-o). Besides, brain lysates showed that these three target genes were
159 down-regulated in corresponding death groups (Fig. 2p-r). Taken together, these data suggested
160 that RfxCas13d mediated mouse death was not due to the loss of target gene function.

161

162 **RfxCas13d mediated lethality was not caused by off-target effects.**

163 One ongoing concern using any CRISPR-Cas system for gene editing is off-target effects^[26].
164 Thus, it's necessary to determine whether RfxCas13d-mediated mouse death is caused by
165 off-target effects. Firstly, Ai14 (Rosa-CAG-LSL-tdTomato-WPRE) reporter mice were introduced
166 and crossed with ^{LSL}RfxCas13d mice to generate ^{LSL}RfxCas13d^{+/-}Ai14^{+/-} mice^[27] (Fig. S3a-b). We
167 designed seven crRNAs targeting tdTomato and tested their knockdown efficiency in N2a cells
168 stably expressing tdTomato by RT-qPCR. Among these crRNAs, crRNA 4 and 7 significantly
169 damped the expression of tdTomato (Fig. 3a). Transcriptome analysis showed that tdTomato was
170 specifically knocked down in cells transfected with tdTomato crRNA 4 or 7 (Fig. 3b). Moreover,
171 the expression of the reported lethal genes was not affected by these two crRNAs. Then, we
172 knocked down tdTomato in ^{LSL}RfxCas13d^{+/-}Ai14^{+/-} mice in the same way as knocking down
173 *Sik3-S*. Results showed that mice injected with AAV-PHP.eB carrying tdTomato crRNA 7 began to
174 lose weight at ~12 dpi and died at ~15 dpi, mice in the other groups behaved normally and
175 survived (Fig. 3c-d). Brain lysates showed that tdTomato expression was lower in tdTomato
176 crRNA 7 group than NT crRNA or tdTomato crRNA 4 group (Fig. 3e).

177 Next, we simultaneously injected AAV-PHP.eB carrying tdTomato crRNA 4, 7 or NT crRNA
178 into ^{LSL}RfxCas13d and ^{LSL}RfxCas13d^{+/-}Ai14^{+/-} mice. Theoretically, if RfxCas13d-mediated
179 mouse death was caused by off-target effects, both ^{LSL}RfxCas13d and ^{LSL}RfxCas13d^{+/-}Ai14^{+/-}
180 mice injected with AAV-PHP.eB carrying tdTomato crRNA 7 would die. However, if
181 RfxCas13d-mediated mouse death was not caused by off-target effects, only
182 ^{LSL}RfxCas13d^{+/-}Ai14^{+/-} mice injected with AAV-PHP.eB carrying tdTomato crRNA 7 would die
183 (Fig. 3f). Results showed that only ^{LSL}RfxCas13d^{+/-}Ai14^{+/-} mice injected with AAV-PHP.eB
184 carrying tdTomato crRNA 7 began to lose body weight at ~12 dpi and died at ~15 dpi, mice in the
185 other groups behaved normally (Fig. 3g-h). These data suggested that RfxCas13d-mediated mouse
186 death was not caused by off-target effects. Moreover, since tdTomato is a foreign gene and has no
187 function in brain neurons, this result further support that RfxCas13d mediated lethality had
188 nothing to do with the loss of target gene function.

189

190 **The collateral activity of RfxCas13d was determined by the abundance of target RNA in**
191 **mammalian cells.**

192 Above data ruled out the possibility that the death of mice was caused by the loss of target gene
193 function or off-target effects. In addition, interestingly, only when the target genes were present
194 and obviously knocked down, the mice would die. It was reminiscent of collateral activity of
195 Cas13. Firstly, we verified findings in previous studies^[14, 17]. We transfected *in vitro*-synthesized
196 EGFP crRNA or NT crRNA into U87 cells stably expressing LwaCas13a and EGFP. The protein
197 sequence of LwaCas13a and the sequence of crRNA we used are the same as previously
198 reported^[14]. Results showed that EGFP mRNA was significantly knocked down at 4 h and 8 h post
199 transfection of EGFP crRNA, not NT crRNA (Fig. S4a). RNA denaturing gel electrophoresis of
200 total RNA showed that 28s and 18s rRNAs were intact, and not cleaved into multiple bands as
201 previous reported (Fig. S4b). Gootenberg and Abudayyeh group reported that LwaCas13a,
202 PspCas13b and RfxCas13d exhibit collateral activity in U87 cells, thereby reducing cell
203 viability^[17]. But according to their results, transfection of plasmids encoding LwaCas13a,
204 PspCas13b or RfxCas13d into U87 cells, regardless of with targeting or NT crRNA, would affect
205 cell viability, indicating that cell viability changes have nothing to do with collateral activity.
206 Therefore, it is still unclear whether collateral activity of Cas13 exists in mammalian cells.

207 We transiently transfected plasmids encoding RfxCas13d, tdTomato and crRNAs into
208 HEK293T cells. Results showed that the protein and RNA level of RfxCas13d decreased, when it
209 knocked down tdTomato under guidance of tdTomato crRNAs not NT crRNA (Fig. 4a-b).
210 However, this phenomenon would not occur when there was no target gene expression or using
211 catalytically dead RfxCas13d (dRfxCas13d) (Fig. 4a-b). This suggested that the collateral activity
212 of RfxCas13d was activated to cleave its own mRNA when RfxCas13d-crRNA complex bound
213 and cleaved tdTomato mRNA. Interestingly, changes in protein levels were more obvious than
214 changes in RNA levels (this will be explained later). The same phenomenon was observed when
215 knocking down *Sik3-S* (Fig. S4c-d). LwaCas13a and PspCas13b also exhibited similar
216 characteristics (Fig. S4e-f). Yang group found that LwaCas13a, RfxCas13d and Cas13X.1
217 exhibited collateral activity when targeting transiently overexpressing mCherry, but not
218 endogenous genes, using EGFP stably expressed in HEK293T as the indicator of collateral
219 effects^[10], which gives us a hint that collateral activity of Cas13 may relates with the abundance of
220 target RNA. Besides, in bacteria, Cas13-induced dormancy requires target RNA levels to exceed
221 an expression threshold^[28]. And *in vitro* experiments proved that collateral activity of Cas13 is
222 positively correlated with the abundance of target RNA^[5, 29]. To verify whether this correlation is
223 also present in mammalian cells, a HEK293T cell line inducibly expressing tdTomato was
224 constructed leveraging the tetracycline-controlled Tet-On inducible expression system, and then
225 transfected with plasmids encoding RfxCas13d and crRNAs under different concentration
226 doxycycline treatment (Fig. 4c). Results showed that RfxCas13d was negatively correlated with
227 tdTomato at the expression level, under co-transfection of RfxCas13d and tdTomato crRNAs
228 instead of NT crRNA (Fig. 4c). These data indicated that the collateral activity of RfxCas13d was
229 triggered and positively correlated with the abundance of target RNA in mammalian cells, when
230 targeting exogenous genes.

231 Next, we determined whether the collateral activity of RfxCas13d occurs when targeting
232 endogenous genes in mammalian cells. We noticed that these endogenous genes previously used
233 as targets are low in abundance^[8, 10]. It is possible that collateral activity had been activated, but it
234 was too weak to be detected. Therefore, we here selected several highly expressed genes as targets
235 and designed four crRNAs for each gene. Then, plasmids encoding RfxCas13d/dRfxCas13d and
236 crRNAs were transiently transfected into HEK293T cells. The knockdown efficiency of crRNAs
237 was measured by RT-qPCR (Fig. 4d-f and S4g-j), and collateral activity was detected by
238 measuring RfxCas13d expression level (Fig. 4g-i and S4k-n). Results showed that RfxCas13d, not
239 dRfxCas13d, was down-regulated when targeting highly expressed genes, indicating that collateral
240 activity was activated (crRNAs pointed by red arrows in Fig. 4g-i and S4k-n). Taken together,
241 these data demonstrated that RfxCas13d exhibited collateral activity in mammalian cells, which is
242 positively correlated with the abundance of target RNA.
243

244 **The collateral activity of RfxCas13d cleaves 28s rRNA into two fragments, leading to**
245 **translation attenuation and activation of ZAK α -JNK/p38-IEG pathway.**

246 Although it was confirmed that the collateral activity of RfxCas13d existed in mammalian cells.
247 It remains unknown whether and how this activity affects the biological process of cells. To this
248 end, we constructed a HEK293T cell line stably expressing RfxCas13d (HEK293T-RfxCas13d)
249 and then transfected with plasmids encoding target gene and corresponding crRNAs (Fig. S5a). In
250 this way, RfxCas13d was fully expressed before the collateral activity was induced, which
251 prevents the collateral activity of RfxCas13d from affecting its own expression by cleaving
252 RfxCas13d mRNA (Fig. S5b). Thus, more RfxCas13d protein and the secondary induced
253 collateral activity could be preserved than co-transfection. Then, cells were harvested 24 h post
254 transfection for cell cycle distribution analysis, total RNA integrity analysis and RNA-seq (Fig.
255 S5a). Analysis of total RNA integrity showed that, not only 28s and 18s rRNA, two additional
256 bands but also were detected when co-transfecting of target genes and corresponding targeting
257 crRNAs instead of NT crRNA into HEK293T-RfxCas13d cells (Fig. 5a). The same phenomenon
258 occurred when targeting endogenous highly expression genes (Fig. S5c). In terms of size, these
259 two additional bands looked like the products of 28s rRNA being cleaved. To test this, we did
260 oligonucleotide extension assay to map cleavage sites (Fig. S5d). PCR and sanger sequencing
261 revealed that 28s rRNA was cut into two fragments, one fragment of ~2100nt and the other
262 segment of ~2800nt (Fig. S5e-f). Noticeably, several sequencing results detected until ~2187nt of
263 28s rRNA (marked by blue color), and one sequencing result revealed that a poly-A tail was added
264 to 2187nt of 28s rRNA (marked by brown color) (Fig. S5f). There is “UU” behind 2187nt of the
265 complete 28s rRNA (marked by red color) (Fig. S5f). And we proved that the collateral activity of
266 RfxCas13d prefers to cleave poly-U *in vitro*, which is consistent with previous study^[30] (Fig.
267 S5g-h). Therefore, this “UU” site (2188-2189nt) is likely to be the cleavage site by RfxCas13d on
268 28s rRNA (Fig. 5b). Those slightly shorter fragments may be caused by post-cleavage degradation.
269 Interestingly, why did the collateral activity of RfxCas13d cleave 28s rRNA but not 18s rRNA?
270 Theoretically, the abundance of 18s rRNA is also high, and there are also “UU” sites on it that can
271 be cleaved. Besides, why did the collateral activity of RfxCas13d cut 28s rRNA at this “UU” site
272 not others? We speculated that it may be due to the structure of RNA and RNA binding proteins
273 (RBPs) that protect rRNAs from being cut. To test our speculation, we extracted total RNA from
274 HEK293T cells and reconstituted the collateral activity of RfxCas13d *in vitro*, and founded that
275 28s and 18s rRNA were cleaved into multiple fragments (Fig. S5i), indicating that RNA structure
276 and RBPs were involved in protecting RNA from the collateral activity of RfxCas13d. 28s rRNA
277 is an important component of the ribosome. To determine whether the translation function of the
278 ribosome was affected due to 28s rRNA breakage, SUnSET assay was employed to monitor
279 protein synthesis. To avoid the impact of SIK3-S enzyme activity on translation, we used kinase
280 dead SIK3-S (SIK3-S-K37M) instead of WT SIK3-S (Fig. S6a). Results showed that protein
281 synthesis was attenuated when target genes were co-transfected with targeting crRNA, not NT
282 crRNA (Fig. 5c). These data suggested that the collateral activity of RfxCas13d cleaved 28s rRNA
283 into two fragments, thereby affecting the translation function of the ribosome. This may explain
284 why in Fig. 4a, changes in protein levels of RfxCas13d were more obvious than changes in RNA
285 levels (Fig. S5b). Cell cycle distribution analysis showed that co-transfection of target gene and
286 targeting crRNAs, but not NT crRNA led to cell cycle arrest at G1 phase (Fig. 5d and S6b).
287 This may be caused by impaired translation of protein.

288 RNA-seq analysis showed that there were 509 common differentially expressed genes from four
289 sets of comparisons (Fig. 5e). Interestingly, these were all up-regulated genes compared with NT
290 crRNA (Supplementary Table 1). Among these genes, we noticed that multiple genes with obvious
291 difference belong to IEGs (Fig. 5f). Besides, transcription factor enrichment analysis of 509 genes
292 showed that multiple enriched transcription factors mediate the expression of IEGs, including
293 JUNB, FOSB, JUN, EGR1, EGR2, ATF3, NR4A3, NR4A1 and CSRNP1 (Fig. 5g). IEGs are
294 genes which are activated transiently and rapidly in response to various cellular stimuli. There are
295 several pathways that lead to the activation of IEGs, such as the RhoA-actin and the ERK, JNK
296 and p38 MAPK pathways^[31]. We used inhibitors of these pathways to block IEGs expression, and
297 found that IEGs expression can be blocked by p38 and JNK inhibitors not MEK1/2 or RhoA/C
298 inhibitors (Fig. S6c-d). The combination of p38 and JNK inhibitors worked better (Fig. S6c-d).
299 Consistently, western blot revealed increased phosphorylation of p38 and JNK, but not ERK1/2
300 (Fig. 5h), demonstrating that JNK and p38 were responsible for the expression of IEGs. Previous

301 studies reported that ZAK α , the long isoform of ZAK, senses ribotoxic stress caused by rRNA
302 damage or ribosome impairment, and then activates p38 and JNK pathways^[32]. We speculated that
303 ZAK α may sense 28s rRNA breakage caused by RfxCas13d and activate JNK and p38 pathways.
304 To test this, we firstly used two ZAK inhibitors (6p^[33] and HY180) to block IEGs expression.
305 IEGs expression can be inhibited by both inhibitors in a dose-dependent manner (Fig. S6e-f). Then,
306 we knocked out ZAK in HEK293T-RfxCas13d cells and found that IEGs expression was blocked
307 in ZAK knockout cells not PKR (another ribotoxic stress sensor) knockout cells (Fig. 5i-k).
308 Besides, re-expression of ZAK α not ZAK β (the short isoform of ZAK) in ZAK knockout cells can
309 rescue the expression of IEGs (Fig. 5i-k). Consistently, western blot demonstrated that
310 phosphorylation of p38 and JNK was blocked in ZAK knockout cell, and can be rescued by
311 re-expression of ZAK α not ZAK β (Fig. 5l). These data proved that ZAK α sensed 28s rRNA
312 breakage caused by RfxCas13d and mediated phosphorylation of p38 and JNK, then activating
313 IEGs expression. Taken together, these data demonstrated that the collateral activity of RfxCas13d
314 cleaves 28s rRNA into two fragments, leading to translation attenuation and activation of the
315 ZAK α -JNK/p38-IEG pathway (Fig. 5m).
316

317 **Discussion**

318 Here, we initially utilized RfxCas13d to specifically knock down *Sik3-S* in the adult mouse
319 brain neurons for studying its role in sleep. Unexpectedly, mice died when SIK3-S was obviously
320 knocked down, which arises our curiosity about the death of mice. Subsequent *in vivo* experiments
321 ruled out the possibility that RfxCas13d-mediated mouse death was due to loss of gene function or
322 off-target effects, and demonstrated that mice would die when target genes were present and
323 obviously knocked down. These data reminded us whether the death of mice was caused by
324 activation of collateral activity when RfxCas13d recognized and cleaved target genes. To prove
325 this, we confirmed that RfxCas13d exhibits collateral activity in mammalian cells, which is related
326 to the abundance of target genes. Then, we founded that the collateral activity of RfxCas13d
327 cleaves 28s rRNA into two fragments, leading to translation attenuation and activation of ZAK α
328 -JNK/p38-IEG pathway. In conclusion, we found that RfxCas13d exhibits collateral effects in
329 mammalian cells, causing death in mice.

330 Previous studies used RfxCas13d to knock down endogenous genes *in vivo*, such as in brain glia,
331 liver and eyes, without side-effect reported. But we observed mouse death when using RfxCas13d
332 to knock down endogenous genes in brain neurons. This discrepancy in experimental outcome
333 may be because neurons are more important than other kinds of cells and not easy to regenerate,
334 so neurons are more sensitive to collateral activity, and animal's performance is more obvious. The
335 death of mice warned us that the safety of RfxCas13d needs to carefully evaluation in animal
336 models before applying it to treatment.

337 During the research, we found that exogenous genes were more likely to be cleaved by the
338 collateral activity of RfxCas13d than endogenous genes, which may be due to the fact that
339 endogenous genes hold more comprehensive RNA structure and closer combination with RBPs
340 than exogenous genes. Therefore, changes in the expression of exogenous genes, such as EGFP or
341 mCherry, are more suitable as indicators of the collateral activity of RfxCas13d, but the cleavage
342 of exogenous genes does not represent that endogenous genes will also be cleaved.

343 The cleavage of 28s rRNA was easily observed, due to its high abundance and important role in
344 cells. But it is still unclear whether the collateral activity of RfxCas13d cuts other RNAs. We
345 observed 509 common differentially expressed genes from four sets of comparisons. IEGs are
346 only part of them. It is unclear why other genes were up-regulated, which may be the consequence
347 of the collateral activity of RfxCas13d cleaving RNAs other than 28s rRNA. So, there is an urgent
348 need to establish a method to detect all the cleavage sites of Cas13's collateral activity, which is
349 crucial for Cas13's optimization in the future. When RfxCas13d recognizes and cleaves the target
350 RNA, its collateral activity is activated to cleaves RfxCas13d mRNA and 28s rRNA, which in turn
351 negatively regulates its own expression and collateral activity. Therefore, it is recommended to
352 express Cas13 in cells in advance, and then to induce its collateral activity and study cleavage sites.
353 Studying the cleavage mechanism of Cas13's collateral activity will not only direct Cas13's
354 optimization in transcriptome engineering via reducing or removing collateral activity, but also
355 inspire us to develop new applications in mammalian cells taking advantage of collateral activity.
356

357 **Acknowledgement**

358 This work was supported by the National Key Research and Development Program of China
359 (2016YFA0500300; 2020YFA0707800), the National Natural Science Foundation of China
360 (31570891; 31872736; 32022028; 81991505), Peking University Clinical + X
361 (PKU2020LCXQ009), the Peking University Medicine Fund (PKU2020LCXQ009) and a grant
362 from Zhuhai Science and Technology Innovation Bureau (ZH22036302200063PWC to Z. Yin).
363 Thanks Yichen Deng for help in FCAS. Thanks Prof. Xiaoyun Lu for providing ZAK inhibitors 6p
364 and HY180.

365
366 **Author Contributions**

367 Y.L., J.X., F.Y. and Q.L. conceived the study and analyzed the data. Y.L., J.X. and Z.L. performed
368 most of the experiments. X.G. was responsible for RNA-seq analysis. Y.W., S.L. and L.C. provided
369 advise and technical help. Q.L. was responsible for AAV preparation. S.W. generated
370 ^{LSL}RfxCas13d mice. Y.G., G.W., Z.Z., X.W., Y.Z., T.L., X.W., H.X, M.K., Q.G., J.L. and L.C.
371 assisted in the molecular experiments. Y.L., F.Y. and Q.L. wrote and revised the paper. J.X, S.L.
372 and L.C. helped with the paper revision.

373
374 **Competing Interests**

375 The authors have no conflicts of interest to declare

376 **STAR Methods**

377 **Cell culture**

378 HEK293T, N2a and U87 cells were obtained from ATCC. Cells were cultured in DMEM
379 medium supplemented with 10% FBS (Gibco) and 100 U/ml Penicillin-Streptomycin in a
380 humidified incubator at 37 °C with 5% CO₂. Additional 1% glutamine for U87 cells.

381 **Animals**

382 All animals care and use adhered to the Guide for the Care and Use of Laboratory Animals of
383 the Chinese Association for Laboratory Animal Science. All procedures of animal handling were
384 approved by the Animal Care Committee of Peking University Health Science Center (permit
385 number LA 2016240). ^{LSL}RfxCas13d and Sik3-E5^{fllox} mice on a C57BL/6J background were
386 generated by the Transgenic Animal Center, NIBS, Beijing, China. Ai14 reporter mice were
387 purchased from The Jackson Laboratory. Wild-type mice were purchased from Department of
388 Laboratory Animal Science of Peking University Health Science Center, Beijing, China. Mice
389 were kept and bred in pathogen-free conditions.

390 **Plasmids construction**

391 Plasmids used in this study were prepared by standard molecular biology techniques and coding
392 sequences entirely verified. All the mutants were constructed by standard molecular biology
393 technique. Each mutant was confirmed by sequencing.

394 **Reagents and antibodies**

395 Polyethylenimine (PEI) (764582, Sigma-Aldrich) and jetPRIME (114-15, Polyplus) were used
396 for transfection. *In vitro*-synthesized crRNAs were purchased from GenScript. Quenched
397 fluorescent reporter RNA was purchased from General Biology. Inhibitors used in this study
398 including the following: p38 inhibitor SB203580 (HY-10256, MCE); JNK inhibitor SP600125
399 (HY-12041, MCE); MEK1/2 inhibitor U0126 (HY-12031, MCE); RhoA/C inhibitor (S7719,
400 Selleck). ZAK inhibitors 6P and HY180 are gift from Prof. Xiaoyun Lu, Jinan University.
401 Antibodies used in this study include the following: anti-HA (Rabbit, H6908, Sigma-Aldrich);
402 anti-HA (Mouse, self-made); anti-SIK3 (Rabbit, self-made); anti-β-Tubulin (Mouse, HC101,
403 TransGen Biotech); anti-ACTB (Mouse, 60008-1-Ig, Proteintech); anti-GAPDH (Mouse,
404 60004-1-Ig, Proteintech); anti-NeuN (Rabbit, 26975-1-AP, Proteintech); anti-Tau (Rabbit,
405 10274-1-AP, Proteintech); anti-MAP2 (Rabbit, 17490-1-AP, Proteintech); anti-ZAK (Rabbit,
406 28761-1-AP, Proteintech); anti-PKR (Rabbit, 18244-1-AP, Proteintech); anti-p-p38 (Rabbit, 4511,
407 CST); anti-p-JNK (Rabbit, 4370, CST); anti-p-ERK1/2 (Rabbit, ET1609-42, HUABIO);
408 HRP-conjugated Affinipure Goat Anti-Rabbit IgG(H+L) (SA00001-2, Proteintech);
409 HRP-conjugated Recombinant Rabbit Anti-Mouse IgG Kappa Light Chain (SA00001-1,
410 Proteintech).

411 **AAV-PHP.eB packaging, purification and injection**

412 AAV-PHP.eB was packaged in AAVpro 293T cells (632273, Clontech). PHP.eB
413 (Addgene#103005), pHelper (240071-54, Agilent) and transfer plasmids were co-transfected to
414 AAVpro 293T cells by PEI MAX (24765, Polysciences). Cells were harvested by cell lifter
415 (70-2180, Biologix) 72 h post-transfection. The cell pellets were suspended in 1x Gradient Buffer
416 (10 mM Tris-HCl pH=7.6, 150 mM NaCl, 10 mM MgCl₂). Five repeated cycles of liquid nitrogen
417 freezing, 37°C water bath thawing and vortex were used to lyse cell. Then ≥50 U/ml of Benzonase
418 nuclease (E1014, Milipore) were added to cell lysates and incubated at 37°C for 30 min.
419 Centrifuge the cell lysate at 21,130g for 30 min at 4°C and transfer the supernatant to a pre-build
420 iodixanol (D1556, Optiprep) step gradients (15%, 25%, 40% and 58%) for ultracentrifugation
421 purification. Vacuum centrifuge at 41,000rpm, 4°C for 4 h, the virus particles were in the layer of

422 40% iodixanol gradient. Purified virus were extracted from the 40% virus containing layer by
423 needle and concentrated using Amicon filters (UFC801096, EMD) and formulated in sterile
424 phosphate-buffered saline (PBS) supplemented with 0.01% Pluronic F68 (24040032, Gibco).
425 Virus titers were determined by qPCR while a linearized AAV plasmid as a standard.
426 1×10^{12} vg/mouse AAV-PHP.eB were delivered into mice via retro-orbital injection.

427 **RNA extraction and reverse transcription quantitative real-time PCR (RT-qPCR)**

428 Total RNA from cells were isolated using TRIzol reagent (DP424, TIANGEN). 1ug RNA was
429 reverse transcribed using HiScript II Q RT SuperMix (R223-01, Vazyme). Levels of these
430 indicated genes were analyzed by qPCR amplified using SYBR Green (Q311, Vazyme). Data
431 shown are the relative abundance of the indicated mRNA normalized to ACTB or GAPDH. The
432 primers were list in Table 1.

433 **Measurement of crRNAs' knockdown efficiency**

434 Plasmids encoding RfxCas13d (addgene#109049) and crRNAs (addgene#109053) were
435 transfected into N2a cells. 48 h after transfection, GFP-positive cells were sorted and collected
436 through Fluorescence-Activated Cell Sorting (FACS), and then were extracted for total RNA.
437 Then, levels of indicated genes were measured by RT-qPCR. All crRNAs used in this paper were
438 listed in Table 2.

439 **Cell cycle distribution analysis**

440 Cells were washed and collected using PBS to get rid of serum proteins at centrifugation
441 at 1,200 rpm, 5 min. Resuspend pellet using precooled 70% EtOH solution to fix cells at least 30
442 min at 4°C. The cells can remain in this solution for up to one week. Dilute EtOH/cell suspension
443 with PBS. Spin at 2,000-2,200 rpm for 10 min spin. Cells are much harder to pellet in EtOH. If
444 EtOH is not diluted and the increased rate is not used, significant cell loss will be noticed. Wash
445 cells three times using PBS and then stain cells using DAPI staining solution (C1005, Beyotime)
446 for 30 min. Finally, cells were recorded by Fluorescence Activated Cell Sorting (FACS) and
447 analyzed by FlowJo.

448 **Western Blotting.**

449 Cells were washed with PBS and lysed by incubation on ice for 10 min with RIPA lysis buffer
450 (50 mM Tris, 150 mM NaCl, 0.1% SDS, 0.5% sodium deoxycholate, 1% Triton X-100, protease
451 cocktail [C0001, Targetmol], and 1 mM PMSF). Brain tissue was firstly grinded in a mortar
452 cooled on liquid nitrogen, and then lysed by incubation on ice for 30 min with RIPA lysis buffer.
453 Supernatants were collected by centrifugation at 12,000 rpm for 10 min at 4°C, and then mixed up
454 with loading buffer and boiled for 10 min. Samples were resolved by SDS/PAGE and transferred
455 to 0.22 um nitrocellulose membrane (P-N66485, Pall). The membrane was blocked using skim
456 milk for 30 min, then incubated overnight with primary antibodies, further incubated with the
457 corresponding HRP-conjugated secondary antibodies and finally detected by enhanced
458 chemiluminescence.

459 **SUnSET assay**

460 Cells were incubated with puromycin (2.5 μ g/ml) for 20 min and then washed with ice cold
461 PBS and lysed using RIPA lysis buffer. Equal quantity of cell lysates was submitted to western
462 blot using anti-puromycin antibody to detect protein synthesis. Signals were normalized with
463 probing GAPDH and TUBULIN (loading control).

464 **Construction of Stable and inducible Expression Mammalian Cell Lines**

465 For preparation of lentiviruses, HEK293T cells in 6-well plates were transfected with the
466 lentiviral vector of interest (1,800 ng), the lentiviral packaging plasmids psPAX2 (600 ng) and

467 pMD2.G (600 ng) and 12 μ l of PEI (1 mg/ml). About 48 h after transfection, culture medium
468 containing lentiviruses was collected and centrifugalized at 12,000 rpm for 10 min, and then
469 filtered using 0.22 μ m filter. HEK293T, N2a and U87 cells were then infected at ~50% confluency
470 by lentiviruses for 48 h, followed by selection with puromycin or hygromycin for 7 days.
471 Monoclonal cells were obtained by limiting dilution.

472 **Oligonucleotide extension assay**

473 Total RNA was ligated with oligonucleotide adaptor 1 or 2 respectively using T4 RNA Ligase 1
474 (M0204S, NEB) following manual. Then RNA was purified by ethanol precipitation and then
475 reverse transcribed using R1 or R2 (R312-02, Vazyme). cDNA was amplified by PCR using
476 F1+R1 or F2+R2. PCR products were firstly purified, then linked into T vector (CT101-01,
477 Transgen Biotech), and finally sequenced by sanger sequencing.

478 The sequence of oligonucleotide adapters and primers:

479 adaptor 1 : 5-PO₄-CTGTAGGCACCATCAATGGACCT-NH₂-3 (DNA);

480 adaptor 2 : 5-NH₂-CAGAAGGCACCAACAAAGGACC-OH-3 (RNA);

481 F1: 5-ACCTGGGTATAGGGGCGAAAGAC-3 (DNA)

482 R1: 5-AGGTCCATTGATGGTGCCTACAG-3 (DNA)

483 F2: 5-CAGAAGGCACCAACAAAGGACC-3 (DNA)

484 R2: 5-CCCTTAGAGCCAATCCTTATCCC-3 (DNA)

485 **Reconstitution of the collateral activity of RfxCas13d *in vitro***

486 To detect the collateral activity of RfxCas13d *in vitro*, we performed *in vitro* cleavage assay with
487 100 ng purified RfxCas13d protein, 100 ng synthesized tdTomato RNA, 100 ng crRNA, 2 μ l
488 RNase inhibitor (New England Biolabs), and 200 ng quenched fluorescent RNA reporters (6 nt
489 polyA/U/G/C), in 100 μ l reaction buffer (40 mM Tris-HCl, 60 mM NaCl, 6 mM MgCl₂, pH 7.6)^[5].
490 Reactions were incubated at 37°C for 1 h and measured the fluorescence of RNA reporters with
491 microplate reader. In Fig. S5I, quenched fluorescent RNA reporters were replaced with total RNA
492 extracted from HEK293T cells. Reactions were incubated at 37°C for 1 h and then RNA was
493 purified by ethanol precipitation and quantified by Agilent 2200 Bioanalyzer.

494 **RNA denaturing gel electrophoresis**

495 Make gel: Weigh 0.5 g of agarose powder, add it to 36.5 ml of DEPC water, and heat to
496 completely dissolve the agarose. After cooling slightly (60-70°C), add 5 ml of 10x MOPS
497 Running Buffer (C516042-0001, Sangon Biotech), 8.5 ml of 37% formaldehyde. Then pour the
498 gel in the glue tank, insert the comb, and place it horizontally for use after solidification. Add
499 samples: Mix the following reagents in a clean small centrifuge tube: 2 μ l 10x MOPS Running
500 buffer, 3.5 μ l formaldehyde, 10 μ l formamide (deionized), 4.5 μ l RNA sample. Mix well, keep it at
501 60°C for 10 min, and cool quickly on ice. Add 3 μ l of 10x loading buffer (B548318-0001, Sangon
502 Biotech) and 0.5 μ l of ethidium bromide, then mix well and add an appropriate amount to the
503 sample well of the gel. Electrophoresis: Turn on the electrophoresis instrument, and stabilize the
504 electrophoresis at 7.5 V/cm.

505 **Total RNA integrity analysis**

506 Total RNA was extracted from cells and then quantified by Agilent 2200 Bioanalyzer.

507 **RNA-seq analysis**

508 The sequencing data generated by illumina Noveseq PE150 in fastq file format was filtered by
509 FastQC(<https://www.bioinformatics.babraham.ac.uk/projects/fastqc/>) and
510 Trim-Galore(https://www.bioinformatics.babraham.ac.uk/projects/trim_galore/) softwares for
511 quality control. Then the mouse genome version mm10 and the human genome version hg38 were

512 used as reference genome to align the clean data with Subread software
513 (<http://subread.sourceforge.net/>). The gene count matrix was calculated by the featureCounts
514 (<http://subread.sourceforge.net/>) program. Then the gene count data was normalized using the
515 FPKM formula. The differentially expressed genes were analysed by R package DESeq2
516 (<https://bioconductor.org/packages/release/bioc/vignettes/DESeq2/inst/doc/DESeq2.html>).
517 Transcription factor enrichment analysis was conducted by ChEA3
518 (<https://maayanlab.cloud/chea3/#top>). The raw data and processed data were uploaded to the GEO
519 Datasets (GSE193668).

520 **Statistical Analysis**

521 The descriptive statistical analysis was performed with Prism version 8 (GraphPad Software). All
522 data are presented as mean \pm SEM. A two-tailed Student's t test assuming equal variants was used
523 to compare two groups. In all figures, the statistical significance between the indicated samples
524 and control is designated as *P < 0.05, **P < 0.01, ***P < 0.001, or NS (P > 0.05)

525 **Reference**

- 526 1. Makarova KS, Wolf YI, Iranzo J, Shmakov SA, Alkhnbashi OS, Brouns SJJ, et al.
527 **Evolutionary classification of CRISPR-Cas systems: a burst of class 2 and derived variants.**
528 *Nat Rev Microbiol* 2020; 18(2):67-83.
- 529 2. Shmakov S, Abudayyeh OO, Makarova KS, Wolf YI, Gootenberg JS, Semenova E, et al.
530 **Discovery and Functional Characterization of Diverse Class 2 CRISPR-Cas Systems.** *Mol Cell*
531 2015; 60(3):385-397.
- 532 3. Abudayyeh OO, Gootenberg JS, Essletzbichler P, Han S, Joung J, Belanto JJ, et al. **RNA**
533 **targeting with CRISPR-Cas13.** *Nature* 2017; 550(7675):280-284.
- 534 4. Meeske AJ, Nakandakari-Higa S, Marraffini LA. **Cas13-induced cellular dormancy prevents**
535 **the rise of CRISPR-resistant bacteriophage.** *Nature* 2019; 570(7760):241-245.
- 536 5. Gootenberg JS, Abudayyeh OO, Lee JW, Essletzbichler P, Dy AJ, Joung J, et al. **Nucleic**
537 **acid detection with CRISPR-Cas13a/C2c2.** *Science* 2017; 356(6336):438-442.
- 538 6. Cox DBT, Gootenberg JS, Abudayyeh OO, Franklin B, Kellner MJ, Joung J, et al. **RNA**
539 **editing with CRISPR-Cas13.** *Science* 2017; 358(6366):1019-1027.
- 540 7. Shmakov S, Smargon A, Scott D, Cox D, Pyzocha N, Yan W, et al. **Diversity and evolution**
541 **of class 2 CRISPR-Cas systems.** *Nat Rev Microbiol* 2017; 15(3):169-182.
- 542 8. Konermann S, Lotfy P, Brideau NJ, Oki J, Shokhirev MN, Hsu PD. **Transcriptome**
543 **Engineering with RNA-Targeting Type VI-D CRISPR Effectors.** *Cell* 2018; 173(3):665-676
544 e614.
- 545 9. Yan WX, Chong S, Zhang H, Makarova KS, Koonin EV, Cheng DR, et al. **Cas13d Is a**
546 **Compact RNA-Targeting Type VI CRISPR Effector Positively Modulated by a**

- 547 **WYL-Domain-Containing Accessory Protein.** *Mol Cell* 2018; 70(2):327-339 e325.
- 548 10. Xu C, Zhou Y, Xiao Q, He B, Geng G, Wang Z, et al. **Programmable RNA editing with**
549 **compact CRISPR-Cas13 systems from uncultivated microbes.** *Nat Methods* 2021;
550 18(5):499-506.
- 551 11. Zhou H, Su J, Hu X, Zhou C, Li H, Chen Z, et al. **Glia-to-Neuron Conversion by**
552 **CRISPR-CasRx Alleviates Symptoms of Neurological Disease in Mice.** *Cell* 2020;
553 181(3):590-603 e516.
- 554 12. He B, Peng W, Huang J, Zhang H, Zhou Y, Yang X, et al. **Modulation of metabolic**
555 **functions through Cas13d-mediated gene knockdown in liver.** *Protein Cell* 2020;
556 11(7):518-524.
- 557 13. Zhou C, Hu X, Tang C, Liu W, Wang S, Zhou Y, et al. **CasRx-mediated RNA targeting**
558 **prevents choroidal neovascularization in a mouse model of age-related macular degeneration.**
559 *Natl Sci Rev* 2020; 7(5):835-837.
- 560 14. Wang Q, Liu X, Zhou J, Yang C, Wang G, Tan Y, et al. **The CRISPR-Cas13a Gene-Editing**
561 **System Induces Collateral Cleavage of RNA in Glioma Cells.** *Adv Sci (Weinh)* 2019;
562 6(20):1901299.
- 563 15. Zhang Z, Wang Q, Liu Q, Zheng Y, Zheng C, Yi K, et al. **Dual-Locking Nanoparticles**
564 **Disrupt the PD-1/PD-L1 Pathway for Efficient Cancer Immunotherapy.** *Adv Mater* 2019;
565 31(51):e1905751.
- 566 16. Wang L, Zhou J, Wang Q, Wang Y, Kang C. **Rapid design and development of**
567 **CRISPR-Cas13a targeting SARS-CoV-2 spike protein.** *Theranostics* 2021; 11(2):649-664.

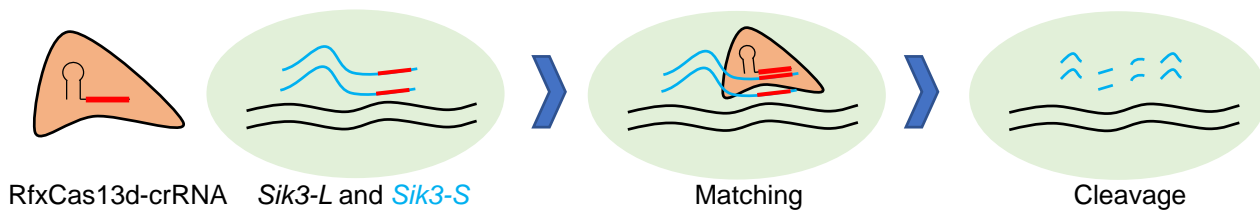
- 568 17. Ozcan A, Krajcski R, Ioannidi E, Lee B, Gardner A, Makarova KS, et al. **Programmable**
569 **RNA targeting with the single-protein CRISPR effector Cas7-11.** *Nature* 2021;
570 597(7878):720-725.
- 571 18. Funato H, Miyoshi C, Fujiyama T, Kanda T, Sato M, Wang Z, et al. **Forward-genetics**
572 **analysis of sleep in randomly mutagenized mice.** *Nature* 2016; 539(7629):378-383.
- 573 19. Wang G, Li Q, Xu J, Zhao S, Zhou R, Chen Z, et al. 2021.
- 574 20. Chan KY, Jang MJ, Yoo BB, Greenbaum A, Ravi N, Wu WL, et al. **Engineered AAVs for**
575 **efficient noninvasive gene delivery to the central and peripheral nervous systems.** *Nat*
576 *Neurosci* 2017; 20(8):1172-1179.
- 577 21. Sasagawa S, Takemori H, Uebi T, Ikegami D, Hiramatsu K, Ikegawa S, et al. **SIK3 is**
578 **essential for chondrocyte hypertrophy during skeletal development in mice.** *Development*
579 2012; 139(6):1153-1163.
- 580 22. Hayasaka N, Hirano A, Miyoshi Y, Tokuda IT, Yoshitane H, Matsuda J, et al. **Salt-inducible**
581 **kinase 3 regulates the mammalian circadian clock by destabilizing PER2 protein.** *Elife* 2017; 6.
- 582 23. Wang HY, Hsieh PF, Huang DF, Chin PS, Chou CH, Tung CC, et al. **RBFOX3/NeuN is**
583 **Required for Hippocampal Circuit Balance and Function.** *Sci Rep* 2015; 5:17383.
- 584 24. Teng J, Takei Y, Harada A, Nakata T, Chen J, Hirokawa N. **Synergistic effects of MAP2**
585 **and MAP1B knockout in neuronal migration, dendritic outgrowth, and microtubule organization.**
586 *J Cell Biol* 2001; 155(1):65-76.
- 587 25. Gumucio A, Lannfelt L, Nilsson LN. **Lack of exon 10 in the murine tau gene results in mild**
588 **sensorimotor defects with aging.** *BMC Neurosci* 2013; 14:148.

-
- 589 26. Vicente MM, Chaves-Ferreira M, Jorge JMP, Proenca JT, Barreto VM. **The Off-Targets of**
590 **Clustered Regularly Interspaced Short Palindromic Repeats Gene Editing.** *Front Cell Dev Biol*
591 2021; 9:718466.
- 592 27. Madisen L, Zwingman TA, Sunkin SM, Oh SW, Zariwala HA, Gu H, et al. **A robust and**
593 **high-throughput Cre reporting and characterization system for the whole mouse brain.** *Nat*
594 *Neurosci*2010; 13(1):133-140.
- 595 28. Vialeto E, Yu Y, Collins SP, Wandera KG, Barquist L, Beisel CL. 2021.
- 596 29. East-Seletsky A, O'Connell MR, Knight SC, Burstein D, Cate JH, Tjian R, et al. **Two distinct**
597 **RNase activities of CRISPR-C2c2 enable guide-RNA processing and RNA detection.** *Nature*
598 2016; 538(7624):270-273.
- 599 30. Brogan DJ, Chaverra-Rodriguez D, Lin CP, Smidler AL, Yang T, Alcantara LM, et al. **A**
600 **Sensitive, Rapid, and Portable CasRx-based Diagnostic Assay for SARS-CoV-2.** *medRxiv*
601 2020.
- 602 31. Bahrami S, Drablos F. **Gene regulation in the immediate-early response process.** *Adv Biol*
603 *Regul*2016; 62:37-49.
- 604 32. Vind AC, Genzor AV, Bekker-Jensen S. **Ribosomal stress-surveillance: three pathways is**
605 **a magic number.** *Nucleic Acids Res*2020; 48(19):10648-10661.
- 606 33. Yang J, Shibu MA, Kong L, Luo J, BadrealamKhan F, Huang Y, et al. **Design, Synthesis,**
607 **and Structure-Activity Relationships of 1,2,3-Triazole Benzenesulfonamides as New Selective**
608 **Leucine-Zipper and Sterile-alpha Motif Kinase (ZAK) Inhibitors.** *J Med Chem* 2020;
609 63(5):2114-2130.

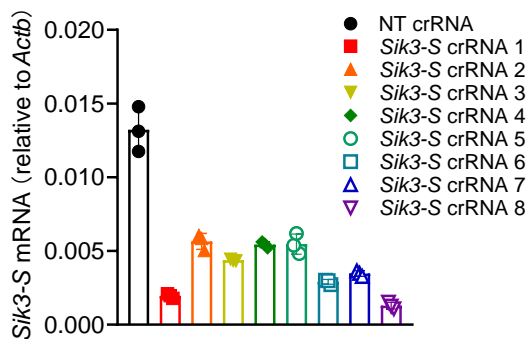
610

Figure 1

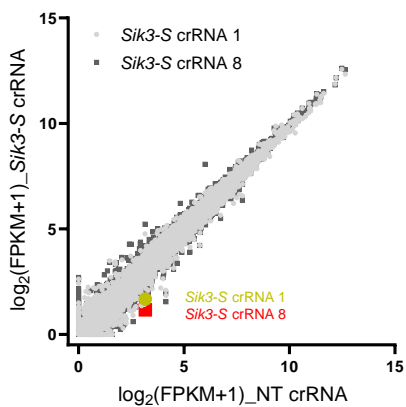
a



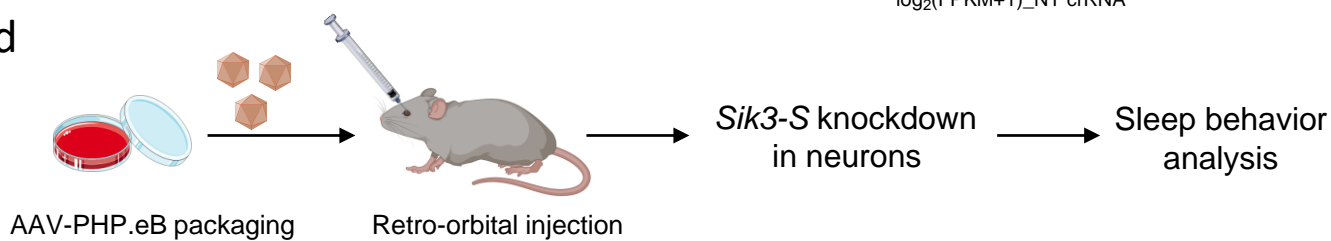
b



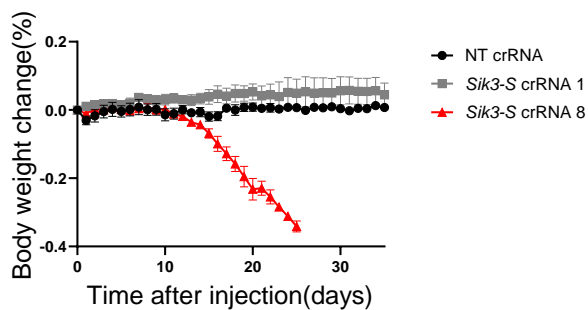
c



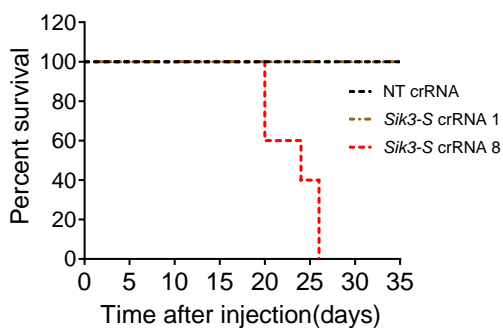
d



e



f



g

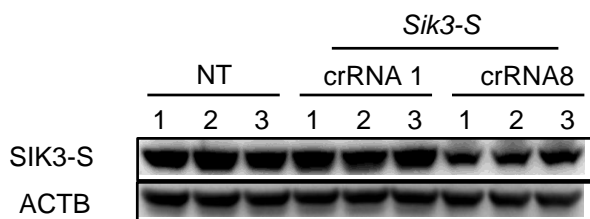
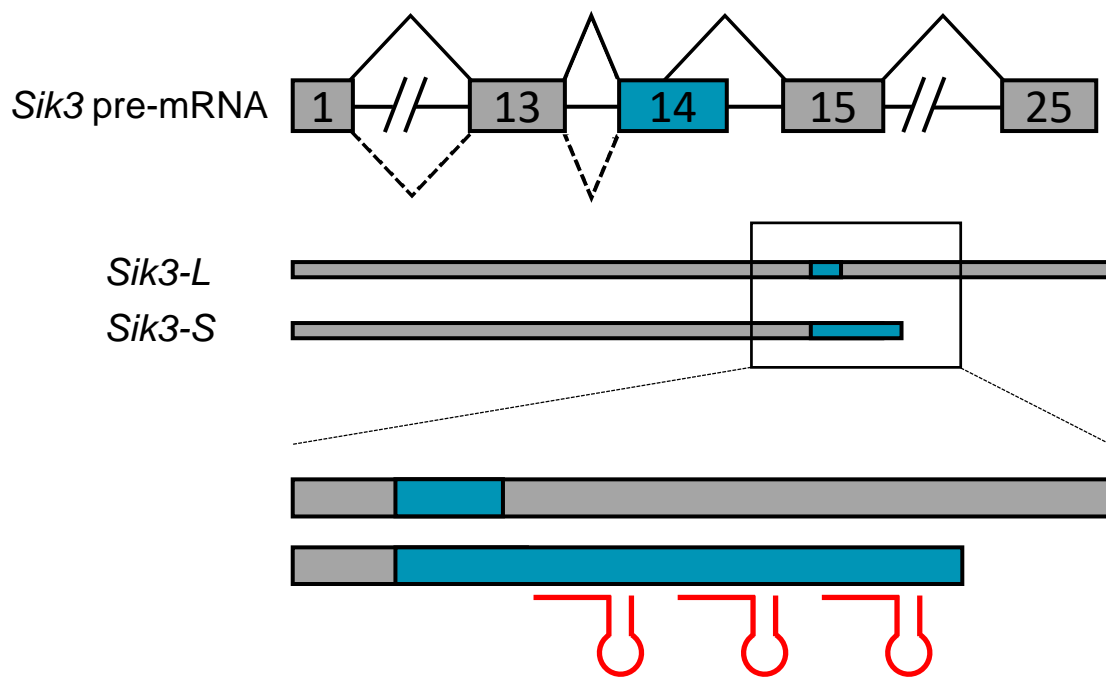
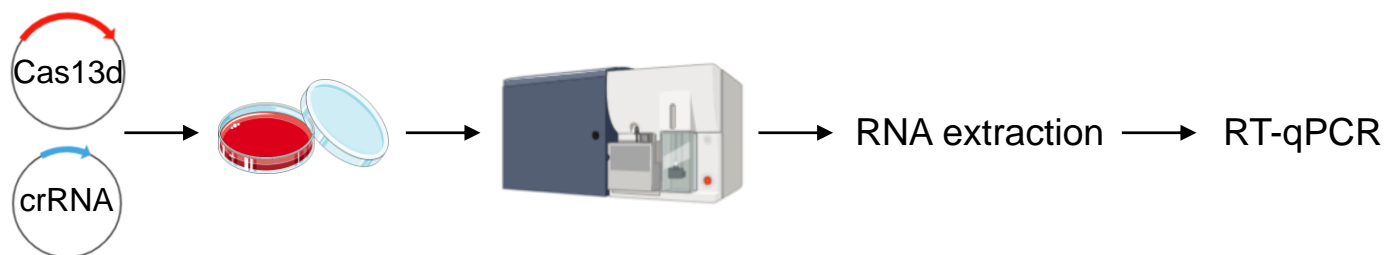


Figure S1

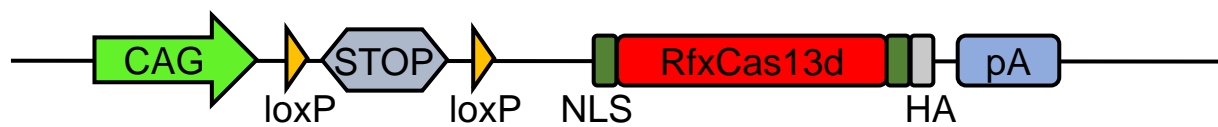
a



b



c



d

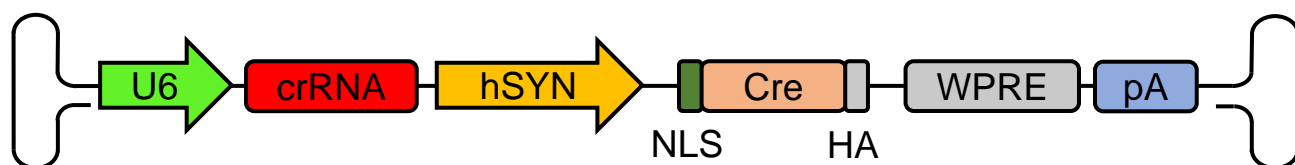


Figure 2

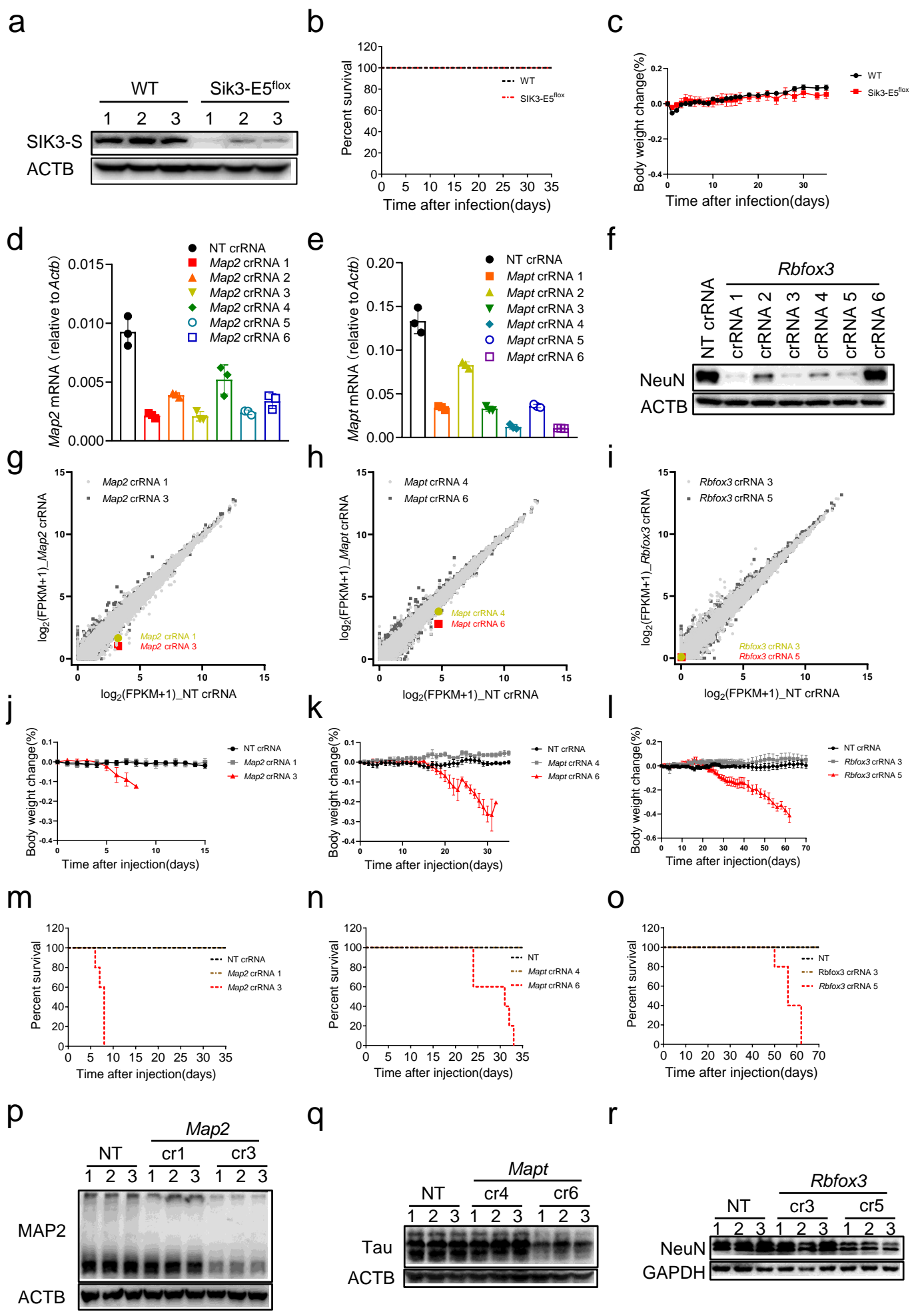
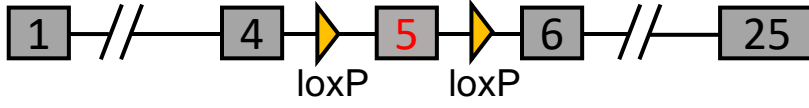


Figure S2

a

Sik3-E5^{lox} locus



AAV-PHP.eB-hSYN-Cre

Sik3-E5^Δ locus

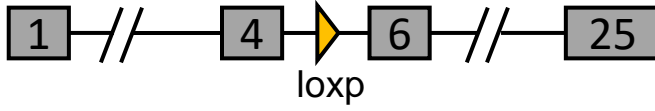


Figure 3

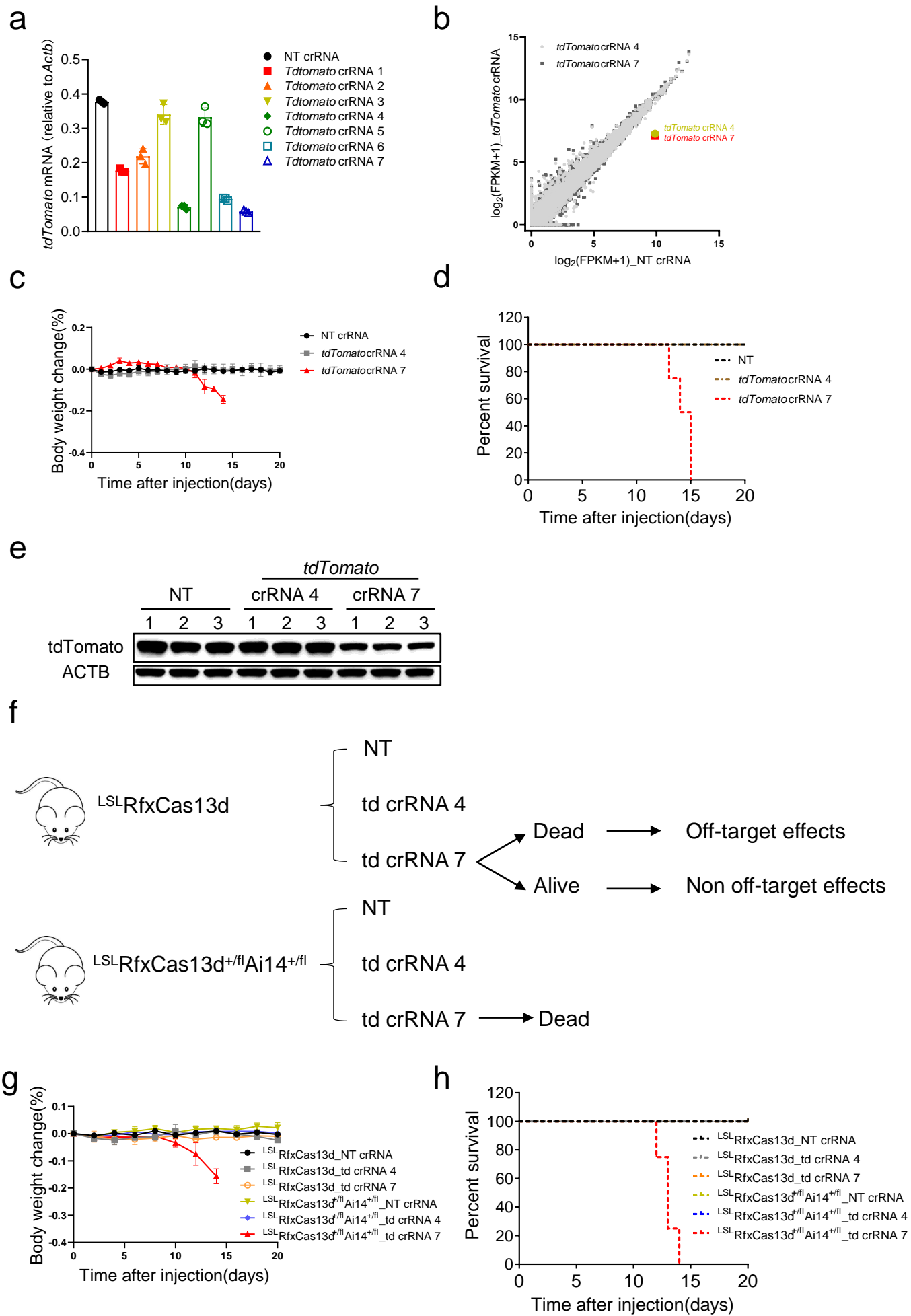


Figure S3

a



b

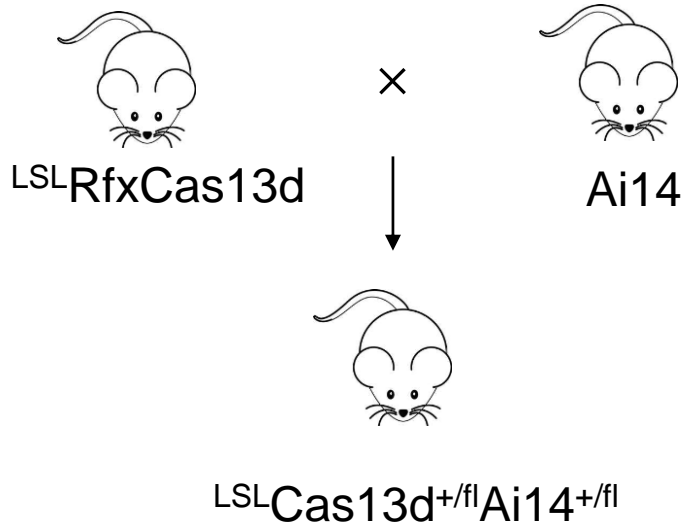


Figure 4

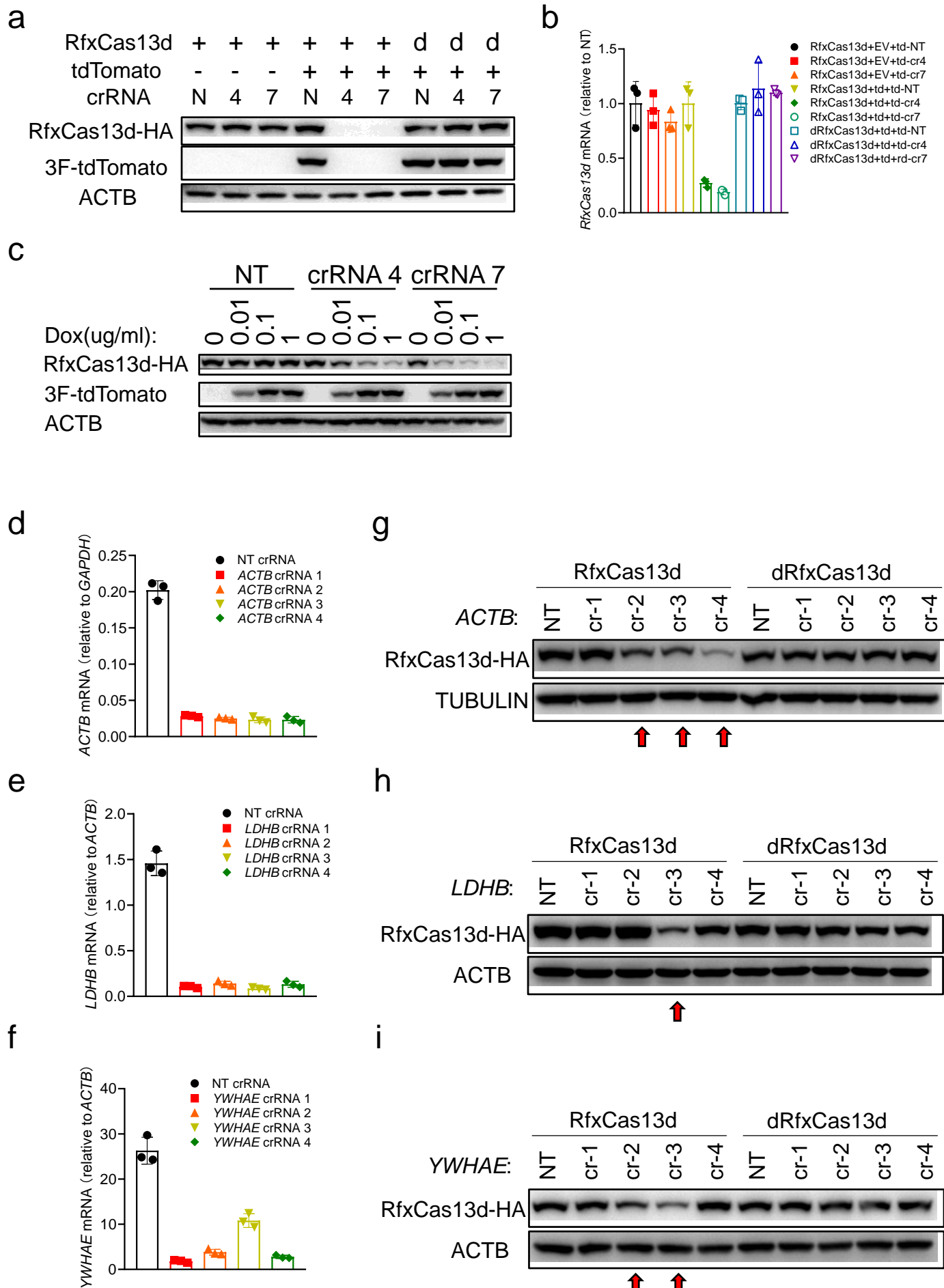


Figure S4

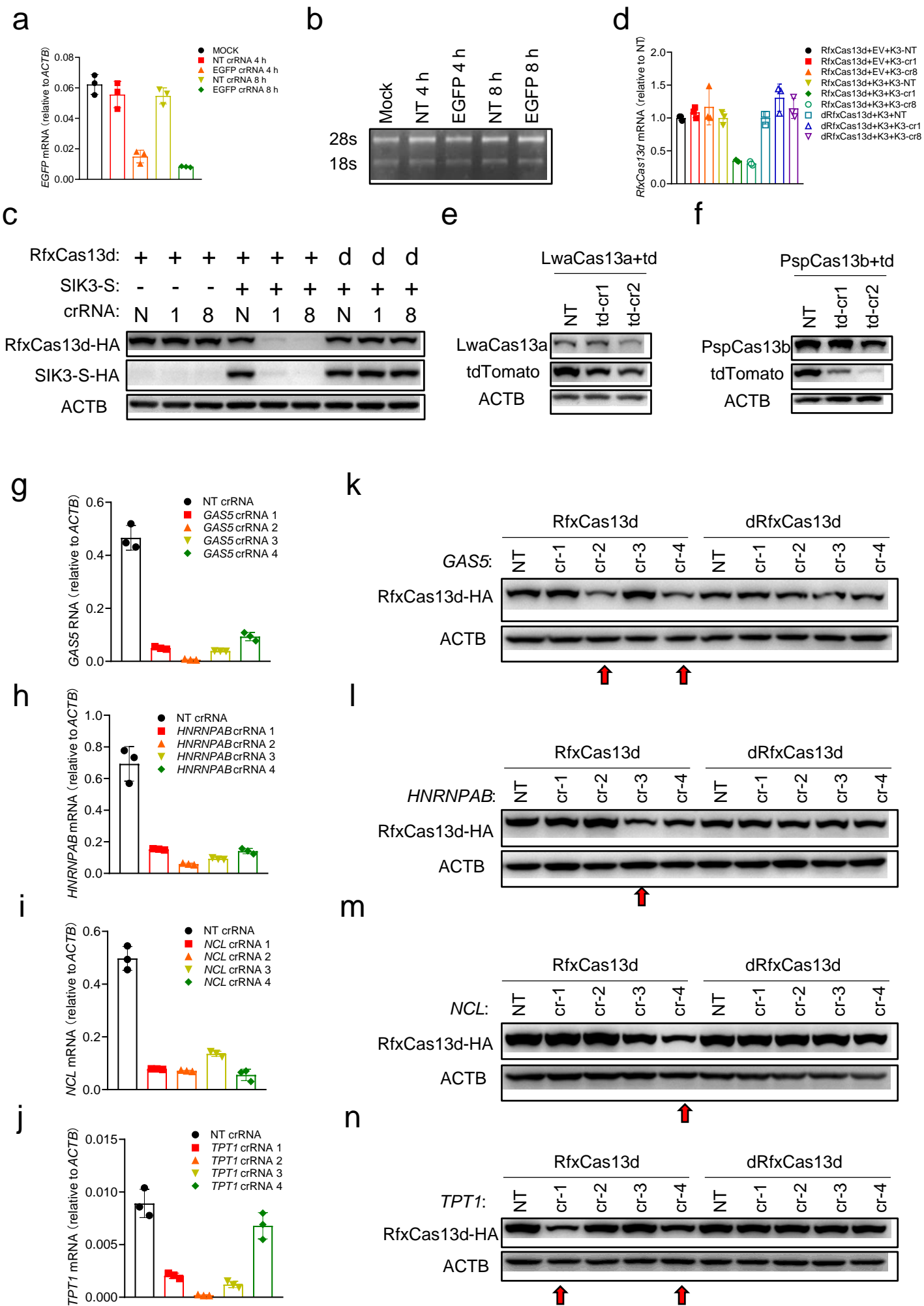


Figure 5

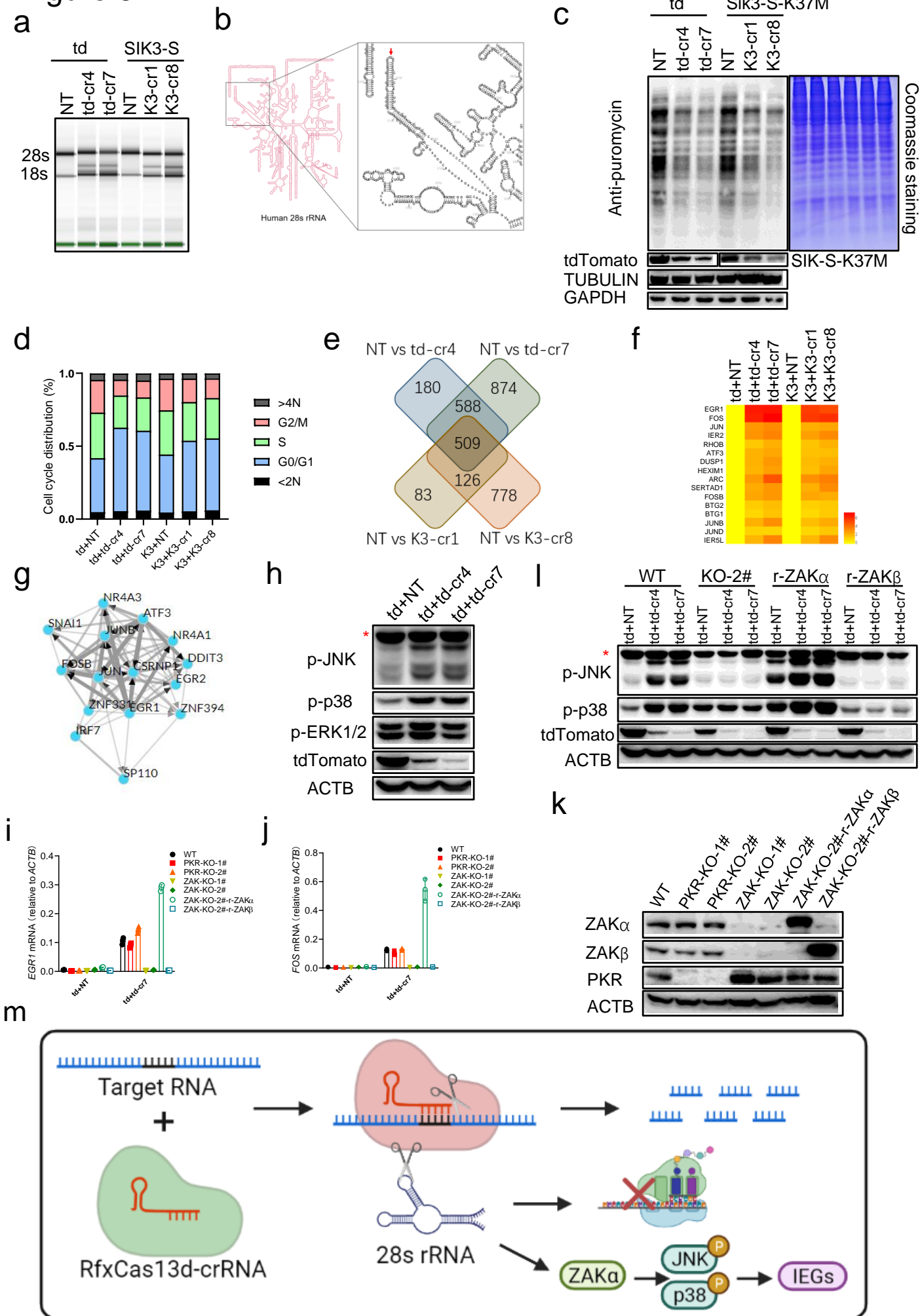
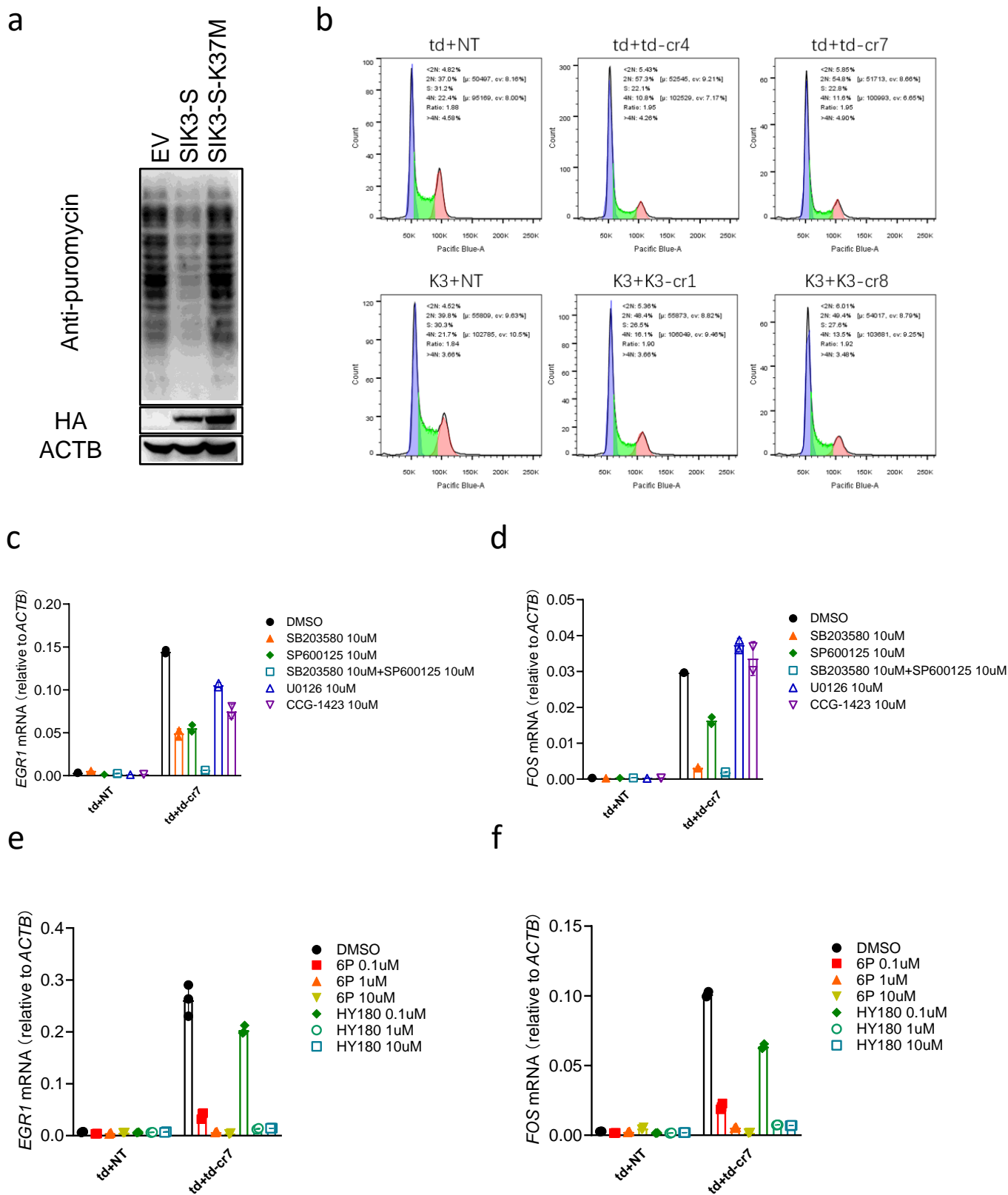


Figure S6



1 **Figure legend**

2 **Figure 1. Mice died when knocking down *Sik3-S* in neurons using RfxCas13d.**

- 3 a. Schematic illustration of RfxCas13d-mediated specifically knockdown of *Sik3-S* not *Sik3-L*
4 mRNA. *Sik3-L*: a transcript encoding a long isoform of SIK3.
5 b. RT-qPCR to measure the knockdown efficiency of *Sik3-S* crRNAs.
6 c. Transcriptome analysis in N2a cells 48 h post transfection of plasmids encoding RfxCas13d and
7 *Sik3-S* crRNAs or NT crRNA. (n=3)
8 d. Workflow of knocking down *Sik3-S* in the adult mouse brain neurons.
9 e. Body weight change curve of ^{LSL}RfxCas13d mice after injection of AAV-PHP.eB carrying
10 *Sik3-S* crRNAs or NT crRNA. (n=5)
11 f. Survival curve of ^{LSL}RfxCas13d mice after injection of AAV-PHP.eB carrying *Sik3-S* crRNAs or
12 NT crRNA. (n=5)
13 g. Western blot to measure SIK-S expression level in brain lysates of ^{LSL}RfxCas13d mice injected
14 with AAV-PHP.eB carrying *Sik3-S* crRNAs or NT crRNA at 20 dpi.

15

16 **Figure S1. Mice died when knocking down *Sik3-S* in neurons using RfxCas13d.**

17 **Linked to Figure 1.**

- 18 a. Schematic illustration of alternative splicing process to generate *Sik3-L* and *Sik3-S* transcripts,
19 and design of *Sik3-S* crRNAs.
20 b. Workflow of measuring the knockdown efficiency of crRNAs in N2a or HEK293T cells.
21 c. Schematic diagram of ^{LSL}RfxCas13d mice. NLS: nuclear localization sequence; HA:
22 hemagglutinin tag; CAG: CAG promoter; U6: U6 promoter; STOP: a tripartite transcriptional
23 stop cassette.
24 d. Schematic illustration of AAV-PHP.eB plasmid used. hSYN: human synapsin 1 gene promoter.

25

26 **Figure 2. RfxCas13d mediated lethality was not due to the loss of target gene function.**

- 27 a. Western blot to measure SIK3-S expression level in brain lysates from *Sik3-E5^{flox}* and WT mice
28 at 21 dpi.
29 b. Survival curve of *Sik3-E5^{flox}* and WT mice after injection of AAV-PHP.eB-hSYN-Cre. (n=5)
30 c. Body weight change curve of *Sik3-E5^{flox}* and WT mice after injection of
31 AAV-PHP.eB-hSYN-Cre. (n=5)
32 d-e. RT-qPCR to measure the knockdown efficiency of *Mapt* and *Map2* crRNAs in N2a cells.
33 f. Western blot to measure the knockdown efficiency of *Rbfox3* crRNAs by knocking down
34 overexpressing NeuN in HEK293T cells using RfxCas13d.
35 g-i. Transcriptome analysis in N2a cells 48 h after transfection of plasmids encoding RfxCas13d
36 and crRNAs. (n=3)
37 j-l. Body weight change curve of ^{LSL}RfxCas13d mice after infection of PHP.eB carrying *Map2*
38 crRNAs, *Mapt* crRNAs or *Rbfox3* crRNAs. (n=5)
39 m-o. Survival curve of ^{LSL}RfxCas13d mice after injection of AAV-PHP.eB carrying *Map2* crRNAs,
40 *Mapt* crRNAs or *Rbfox3* crRNAs. (n=5)
41 p-r. Western blot to measure MAP2 (at 6 dpi), Tau (at 25 dpi) or NeuN (at 50 dpi) expression level
42 in brain lysates of ^{LSL}RfxCas13d mice after injection of AAV-PHP.eB carrying *Map2* crRNAs,
43 *Mapt* crRNAs or *Rbfox3* crRNAs.

44

45 **Figure S2. RfxCas13d mediated lethality was not due to the loss of target gene function.**

46 **Linked to Figure 2.**

47 a. Schematic illustration of knocking out Sik3 by AAV-PHP.eB-hSYN-Cre injection of Sik3-E5^{fllox}
48 mice.

49

50 **Figure 3. RfxCas13d mediated lethality was not caused by off-target effects.**

51 a. RT-qPCR to measure the knockdown efficiency of tdTomato crRNAs in N2a cells stably
52 expressing tdTomato (N2a-td).

53 b. Transcriptome analysis of N2a-td cells 48 h after transfection of plasmids encoding RfxCas13d
54 and tdTomato crRNAs or NT crRNA. (n=3)

55 c. Body weight change curve of ^{LSL}RfxCas13d^{+fl}Ai14^{+fl} mice after injection of AAV-PHP.eB
56 carrying tdTomato crRNAs or NT crRNA. (n=4)

57 d. Survival curve of ^{LSL}RfxCas13d^{+fl}Ai14^{+fl} mice after injection of AAV-PHP.eB carrying
58 tdTomato crRNAs or NT crRNA. (n=4)

59 e. Western blot to measure tdTomato expression level in brain lysates of ^{LSL}RfxCas13d^{+fl}Ai14^{+fl}
60 mice injected with AAV-PHP.eB carrying tdTomato crRNAs or NT crRNA at 12 dpi.

61 f. Schematic of delivering AAV-PHP.eB carrying tdTomato crRNAs or NT crRNA into
62 ^{LSL}RfxCas13d^{+fl}Ai14^{+fl} and ^{LSL}RfxCas13d mice, and the possible outcomes.

63 g. Body weight change curve of ^{LSL}RfxCas13d and ^{LSL}RfxCas13d^{+fl}Ai14^{+fl} mice after injection of
64 AAV-PHP.eB carrying tdTomato crRNAs or NT crRNA. (n=4)

65 h. Survival curve of ^{LSL}RfxCas13d and ^{LSL}RfxCas13d^{+fl}Ai14^{+fl} mice after injection of
66 AAV-PHP.eB carrying tdTomato crRNAs or NT crRNA. (n=4)

67

68 **Figure S3. RfxCas13d mediated lethality was not caused by off-target effects.**

69 **Linked to Figure 3.**

70 a. Schematic diagram of Ai14 reporter mice

71 b. Schematic illustration of generating ^{LSL}RfxCas13d^{+fl}Ai14^{+fl} mice by crossing ^{LSL}RfxCas13d mice
72 with Ai14 mice.

73

74 **Figure 4. The collateral activity of RfxCas13d was determined by the abundance of target
75 RNA in mammalian cells.**

76 a. Western blot to measure the expression level of RfxCas13d and tdTomato 24 h after transfection
77 plasmids encoding RfxCas13d, tdTomato and crRNAs into HEK293T cells. 3F-tdTomato
78 means tdTomato with 3x Flag tag at N-terminal.

79 b. RT-qPCR to measure the RNA level of RfxCas13d in a. td represents tdTomato. EV represents
80 empty vector.

81 c. Western blot to measure the expression level of RfxCas13d and tdTomato 24 h after transfection
82 of plasmids encoding RfxCas13d, tdTomato and crRNAs into inducible-expressing tdTomato
83 HEK293T cells. Cells were treated with different doxycycline concentration in advance.

84 d-f. RT-qPCR to measure the knockdown efficiency of ACTB, LDHB and YEHAЕ crRNAs in
85 HEK293T cells.

86 g-i. Western blot to measure the expression level of RfxCas13d/dRfxCas13d 24 h after
87 transfection of plasmids encoding RfxCas13d/dRfxCas13d and crRNAs into HEK293T cells.
88 cr-1/2/3/4: crRNA 1/2/3/4.

89

90 **Figure S4. The collateral activity of RfxCas13d was determined by the abundance of target**
91 **RNA in mammalian cells.**

92 **Linked to Figure 4.**

93 a. RT-qPCR to measure the RNA level of EGFP after transfecting *in vitro*-synthesized EGFP
94 crRNAs into U87 cells stably expressing LwaCas13a and EGFP.

95 b. RNA denaturing gel to measure the integrity of total RNA in a.

96 c. Western blot to measure the expression level of RfxCas13d and SIK3-S 24 h after transfection
97 plasmids encoding RfxCas13d, SIK3-S and crRNAs into HEK293T cells.

98 d. RT-qPCR to measure the RNA level of RfxCas13d in c. K3 represents SIK3-S; EV represents
99 empty vector.

100 e-f. Western blot to measure the expression level of LwaCas13a/PspCas13b and tdTomato 24 h
101 after transfection of plasmids encoding LwaCas13a/PspCas13b, tdTomato and corresponding
102 crRNAs into HEK293T cells. td-cr1: tdTomato crRNA 1; td-cr2: tdTomato crRNA 2.

103 g-j. RT-qPCR to measure the knockdown efficiency of GAS5, HNRNPAB, NCL and TPT1
104 crRNAs in HEK293T cells

105 k-n. Western blot to measure the expression level of RfxCas13d/dRfxCas13d 24 h after
106 transfection of plasmids encoding RfxCas13d/dRfxCas13d and crRNAs into HEK293T cells.
107 cr-1/2/3/4: crRNA 1/2/3/4.

108

109 **Figure 5. The collateral activity of RfxCas13d cleaves 28s rRNA into two fragments, leading**
110 **to translation attenuation and activation of ZAK α -JNK/p38-IEG pathway.**

111 a. Total RNA of each sample was quantified by Agilent 2200 Bioanalyzer. td: tdTomato; td-cr4/7:
112 tdTomato crRNA 4/7; K3-cr1/8: *Sik3-S* crRNA 1/8.

113 b. Schematic illustration of the cleavage site of RfxCas13d on human 28s rRNA.

114 c. SUNSET assay to measure the protein translation rate of HEK293T-RfxCas13d cells 24 h after
115 transfection of plasmids encoding tdTomato/SIK3-S-K37M and corresponding crRNAs.

116 d. Statistical diagram of cell cycle distribution in Fig. S6b.

117 e. Schematic illustration of 509 common differentially expressed genes from four sets of
118 comparisons.

119 f. Heatmap to demonstrate the expression level of IEGs in different groups. $\log_2(\text{foldchange})$.

120 g. Transcription factor enrichment analysis using ChEA3. There are Top 15 transcription factors.

121 h. Western blot to measure the phosphorylation level of p38, JNK and ERK in
122 HEK293T-RfxCas13d 24 h after transfection of plasmids encoding tdTomato and tdTomato
123 crRNAs or NT crRNA. Red asterisk represents non-specific band.

124 i-j. RT-qPCR to measure the RNA level of EGR1 and FOS in HEK293T-RfxCas13d cells 24 h
125 after transfection of plasmids encoding tdTomato and tdTomato crRNAs or NT crRNA.

126 k. Western blot to measure the expression level of ZAK α , ZAK β and PKR in indicated cells.

127 PKR-KO-1/2#: two strain of PKR knockout HEK293T-RfxCas13d cells; ZAK-KO-1/2#: two

128 strain of ZAK knockout HEK293T-RfxCas13d cells; ZAK-KO-2#-r-ZAK α : re-expression of
129 ZAK α in ZAK-KO-2#; ZAK-KO-2#-r-ZAK β : re-expression of ZAK β in ZAK-KO-2#
130 l. Western blot to measure the phosphorylation level of p38, JNK 24 h after transfection of
131 plasmids encoding RfxCas13d and tdTomato crRNA 7 or NT crRNA into indicated cells. Red
132 asterisk represents non-specific band. KO-2#: ZAK-KO-2#; r-ZAK α : ZAK-KO-2#-r-ZAK α ;
133 r-ZAK β : ZAK-KO-2#-r-ZAK β .
134 m. Schematic illustration that the collateral activity of RfxCas13d cleaves 28s rRNA into two
135 fragments, leading to translation attenuation and activation of ZAK α -p38/JNK-IEGs pathway.
136

137 **Figure S5. The collateral activity of RfxCas13d cleaves 28s rRNA into two fragments,**
138 **leading to translation attenuation and activation of ZAK α -JNK/p38-IEG pathway.**

139 **Linked to Figure 5.**

140 a. Workflow of experiments did in HEK293T-RfxCas13d cells.
141 b. Schematic illustration that the collateral activity of RfxCas13d cleaves its own mRNA and 28s
142 RNA, thereby inhibiting its own protein expression.
143 c. Total RNA of each sample was quantified by Agilent 2200 Bioanalyzer. cr: crRNA.
144 d. Schematic illustration of oligonucleotide extension assay. Red represents oligonucleotide
145 adaptor 1; Yellow represents oligonucleotide adaptor 2.
146 e. Gel picture of PCR products from d.
147 f. Sanger sequencing results. Ref: reference sequence. The numbers in brackets represent the
148 number of identical sequencing results.
149 g. Schematic illustration of reconstitution of the collateral activity of RfxCas13d *in vitro*.
150 h. Statistical diagram of fluorescence intensity in g.
151 i. Total RNA integrity analysis quantified by Agilent 2200 Bioanalyzer.

152

153 **Figure S6. The collateral activity of RfxCas13d cleaves 28s rRNA into two fragments,**
154 **leading to translation attenuation and activation of ZAK α -JNK/p38-IEG pathway.**

155 **Linked to Figure 5.**

156 a. SUNSET essay to measure the protein translation rate of HEK293T-RfxCas13d cells 24 h after
157 transfection of plasmids encoding SIK3-S or SIK3-S-K37M.
158 b. Cell cycle analysis using FCAS.
159 c-d. RT-qPCR to measure the RNA level of EGR1 and FOS in HEK293T-RfxCas13d cells 24 h
160 after transfection of plasmids encoding tdTomato and crRNAs. Inhibitors and transfection mix
161 were added together. SB203580: p38 inhibitor; SP600125: JNK inhibitor; U0126: MEK1/2
162 inhibitor; CCG-1423: RhoA/C inhibitor.
163 e-f. RT-qPCR to measure the RNA level of EGR1 and FOS in HEK293T-RfxCas13d cells 24 h
164 after transfection of plasmids encoding tdTomato and crRNAs into. ZAK inhibitors and
165 transfection mix were added together. 6p and HY180: ZAK inhibitors.
166

Table 1. The sequence of qPCR primers used in this study.

| Gene Name | Species | Forward primer | Reverse primer |
|-----------|---------|-------------------------|---------------------------|
| Sik3-S | Mouse | CAGAGCGACAGTGACCATCA | GCTGGATTCTGGTGAAAACCC |
| Map2 | Mouse | ACCTTCCTCCATCCTCCCTC | TCCTGCTCTGCGAATTGGTT |
| Mapt | Mouse | CCTCCTAGGCCTGACTCCTT | CTGGGGTGGAAGCGAAAGAT |
| Actb | Mouse | TTACGGATGTCAACGTACAGTTC | ACTATTGGCAACGAGCGGTTCT |
| TPT1 | Human | GGACTACCGTGAGGATGGTG | GGATTTCTTTCTTTTGCATCACATT |
| LDHB | Human | GCCTTCTCTCTCCTGTGCAA | CCTCTTCTCCGCAACTGGT |
| NCL | Human | AAGCGTTGGAAGTCACTGGT | TCTCGCATCTCGCTCTTTCT |
| YWHAE | Human | GCAGAACTGGATACGCTGAG | ATTCTGCTCTTACCGTCAC |
| HNRNPAB | Human | TGTCAGTGGAAGCAAGTGTGA | CTGGTTCCAGTAGTTGCCGT |
| GAS5 | Human | TATGGTGCTGGGTGCAGATG | CCATTAAGCTGGTCCAGGCA |
| EGR1 | Human | ACCTGACCGCAGAGTCTTTT | CAAGGTGTTGCCACTGTTGG |
| FOS | Human | TACTCTCAAGCGGAGACAG | TCCTTCAGCAGGTTGGCAAT |
| GAPDH | Human | CAGCCTCAAGATCATCAGCA | TGTGGTCATGAGTCCTTCCA |
| ACTB | Human | AAAGACCTGTACGCCAACAC | GTCATACTCCTGCTTGCTGAT |
| RfxCas13d | | GACCCGTCAGCAGGATATG | AGGCGGCGTTGGTAATGTAT |
| tdTomato | | CCTGTTCTGGGGCATGGCA | TCTTTGATGACGGCCATGTTGTTGT |
| EGFP | | CGTAAACGGCCACAAGTTCA | CTTCATGTGGTCGGGGTAGC |

Table 2. The sequence of crRNAs used in this study.

| Subtypes of Cas13 | crRNA name | Sequence |
|-------------------|------------------|-------------------------|
| RfxCas13d | NT crRNA | TCACCAGAAGCGTACCATACTC |
| RfxCas13d | Rbfox3 crRNA 1 | CTGCATAGAATTCAGGCCATA |
| RfxCas13d | Rbfox3 crRNA 2 | GAAATGTATTATACACAGCACG |
| RfxCas13d | Rbfox3 crRNA 3 | GCCTCCATAAATCTCAGCACCA |
| RfxCas13d | Rbfox3 crRNA 4 | GAGCATATCTGTAAGCTGCATA |
| RfxCas13d | Rbfox3 crRNA 5 | AAATCCATCCTGATACACGACC |
| RfxCas13d | Rbfox3 crRNA 6 | GCAGCAACATTCAATGAGGCCA |
| RfxCas13d | Sik3-S crRNA 1 | CAAGCACTGCCAGGTGCCACAT |
| RfxCas13d | Sik3-S crRNA 2 | GCAGGGGAGCCTGCCCAAGGAC |
| RfxCas13d | Sik3-S crRNA 3 | AATGGCGCTTATAGAAATGAAA |
| RfxCas13d | Sik3-S crRNA 4 | GAAGAGGGAGGGAGGAGAGAAA |
| RfxCas13d | Sik3-S crRNA 5 | TCACAGAAAATAAGAAAGACAA |
| RfxCas13d | Sik3-S crRNA 6 | TCTCCAATCTCCAACCTCTTTT |
| RfxCas13d | Sik3-S crRNA 7 | GGAGATATTCATTCATTCATTC |
| RfxCas13d | Sik3-S crRNA 8 | GTCGCTCTGTGAATCAGGCATC |
| RfxCas13d | Map2 crRNA 1 | ACTCTCAATTTTCACACGTCCA |
| RfxCas13d | Map2 crRNA 2 | TCAATCTTACATTACCACCTC |
| RfxCas13d | Map2 crRNA 3 | GAGCATTGTCAAGTGAGCCAAC |
| RfxCas13d | Map2 crRNA 4 | CTTCGCCTGTTTAAAAGCACCA |
| RfxCas13d | Map2 crRNA 5 | CCATGCAAAAACAGAGCAGAGCG |
| RfxCas13d | Map2 crRNA 6 | AAAGGAGAAGTATTCACAAGCC |
| RfxCas13d | Mapt crRNA 1 | GTGATATTATCCAAGGAGCCAA |
| RfxCas13d | Mapt crRNA 2 | CCACATCCCAGAATACCACCCC |
| RfxCas13d | Mapt crRNA 3 | GCCAAGCATGAGAACAGGCAGA |
| RfxCas13d | Mapt crRNA 4 | CTTAGATAAAAAGAAAAGGCAGA |
| RfxCas13d | Mapt crRNA 5 | AACTACAACGTAACAGGGCGAA |
| RfxCas13d | Mapt crRNA 6 | ATAAAAAGAAAAGGCAGAGGTCC |
| RfxCas13d | tdTomato crRNA 1 | CCCTCGGAGCGCTCGTACTGTT |
| RfxCas13d | tdTomato crRNA 2 | GGTGCCCTCGTAGGGGCGGCC |
| RfxCas13d | tdTomato crRNA 3 | GGGGGACAGGATGTCCCAGGGC |
| RfxCas13d | tdTomato crRNA 4 | AGGAGTCCTGGGTACGGTCAC |
| RfxCas13d | tdTomato crRNA 5 | TCTTGCCATGTAGATGGTCTT |
| RfxCas13d | tdTomato crRNA 6 | CCAGACCGCCGTCCTCGAAGTT |
| RfxCas13d | tdTomato crRNA 7 | GTCACCTTACGCTTGGCGGTCT |
| RfxCas13d | GAS5 crRNA 1 | CACACAGTGTAGTCAAGCCGAC |
| RfxCas13d | GAS5 crRNA 2 | ATAAAAACGTTACCAGGAGCAG |
| RfxCas13d | GAS5 crRNA 3 | AATTTATTAATAATTGGAGACAC |
| RfxCas13d | GAS5 crRNA 4 | ATAAAAACGTTACCAGGAGCAG |
| RfxCas13d | HNRNPAB crRNA 1 | TTATTGTACAGTCAACGACCTC |
| RfxCas13d | HNRNPAB crRNA 2 | CAACTCTGACTCTGACCTCCAC |

| | | |
|-----------|------------------|------------------------------|
| RfxCas13d | HNRNPAB crRNA 3 | CAAACAAAGCATGTGTGCGATC |
| RfxCas13d | HNRNPAB crRNA 4 | CCTGGTAATAAAAATCAGCCCA |
| RfxCas13d | TPT1 crRNA 1 | G TTCATGACAATATCGACACCA |
| RfxCas13d | TPT1 crRNA 2 | AGTCCAATAGAGCAACCATGCC |
| RfxCas13d | TPT1 crRNA 3 | ATTACCATTAACATGCAGCCTA |
| RfxCas13d | TPT1 crRNA 4 | AGCTCAAGATGACATCAGTCCC |
| RfxCas13d | LDHB crRNA 1 | CCACAAGAGCAAGTTCATCAGC |
| RfxCas13d | LDHB crRNA 2 | CCCAGAATGCTGATAGCACACG |
| RfxCas13d | LDHB crRNA 3 | GGATTCAATAAGATCAGCCACA |
| RfxCas13d | LDHB crRNA 4 | CACACTTAATCCAATAGCCCAG |
| RfxCas13d | NCL crRNA 1 | CCAACAAAGAGATTGAAAGCCG |
| RfxCas13d | NCL crRNA 2 | TCCAACAAAGAGATTGAAAGCC |
| RfxCas13d | NCL crRNA 3 | CAGGTAACAGTAAAAACCCAG |
| RfxCas13d | NCL crRNA 4 | GCAAACCTCTATAAATGCATACC |
| RfxCas13d | YWHAE crRNA 1 | CGGAAAAATTGAGAGCAAGACC |
| RfxCas13d | YWHAE crRNA 2 | GTCATTGCAATATCACTAGCAG |
| RfxCas13d | YWHAE crRNA 3 | AATAGAAAACCTTGGACTCGCC |
| RfxCas13d | YWHAE crRNA 4 | CTACTTTCTTCATTGACTCCAC |
| RfxCas13d | ACTB crRNA 1 | TGAAGCTGTAGCCGCGCTCGGT |
| RfxCas13d | ACTB crRNA 2 | TGAACTTTGGGGGATGCTCGCT |
| RfxCas13d | ACTB crRNA 3 | CGTACAGGGATAGCACAGCCTG |
| RfxCas13d | ACTB crRNA 4 | ATCTTGATCTTCATTGTGCTGG |
| | | |
| LwaCas13a | NT crRNA | CAGACTATGCGTCGACAAGCCAGGCATT |
| LwaCas13a | tdTomato crRNA 1 | AAGCGCATGAACTCTTTGATGACCTCCT |
| LwaCas13a | tdTomato crRNA 2 | TAGATGGTCTTGAATCCACCAGGTAGT |
| | | |
| PspCas13b | NT crRNA | GTAATGCCTGGCTTGTGACGCATAGTC |
| PspCas13b | tdTomato crRNA 1 | AGGAGTCCTGGGTACGGTCACCAGACC |
| PspCas13b | tdTomato crRNA 2 | GTCACCTTCAGCTTGGCGGTCTGGGTGC |